PINK1/Parkin-Mediated Mitophagy Ameliorates Mitochondrial Dysfunction in Lacrimal Gland Acinar Cells During Aging

Han Zhao,[1,2] Yue Zhang,[3–6] Yujie Ren,[7] and Wanpeng Wang[3–6]

[1]Department of Ophthalmology, The Second Xiangya Hospital of Central South University, Changsha, Hunan, China
[2]Hunan Clinical Research Center of Ophthalmic Disease, Changsha, Hunan, China
[3]Eye Center of Xiangya Hospital, Central South University, Changsha, China
[4]Hunan Key Laboratory of Ophthalmology, Changsha, China
[5]National Clinical Research Center for Geriatric Disorders, Xiangya Hospital, Changsha, China
[6]National Key Clinical Specialty of Ophthalmology, Xiangya Hospital, Changsha, China
[7]Department of Ophthalmology, Xi'an No. 1 Hospital, Xi'an, China

Correspondence: Wanpeng Wang, Eye Center of Xiangya Hospital, Central South University, No. 87 Xiangya Rd., Changsha 410008, China; wangwanpeng023@csu.edu.cn.

Received: July 10, 2024
Accepted: October 8, 2024
Published: November 6, 2024

Citation: Zhao H, Zhang Y, Ren Y, Wang W. PINK1/Parkin-mediated mitophagy ameliorates mitochondrial dysfunction in lacrimal gland acinar cells during aging. *Invest Ophthalmol Vis Sci*. 2024;65(13):12. https://doi.org/10.1167/iovs.65.13.12

Purpose. Aging alters the function of the lacrimal gland and disrupts the balance of the microenvironment on the ocular surface, eventually leading to aqueous-tear-deficient dry eye. Mitophagy has been reported to play an important role in aging, but the underlying mechanism remains unclear.

Methods. The young (6 weeks) and middle-aged (12 months) male C57BL/6J mice were used in this study, and mitophagy agonist rapamycin and inhibitor Mdivi-1 were used in in vivo experiments. Hematoxylin and eosin, Masson, Oil Red O, and reactive oxygen species (ROS) staining were used to detect histological changes and lipids in lacrimal gland. Changes in the expression of proteins were identified by Western blotting of lacrimal gland lysates. Transmission electron microscopy and immunofluorescence staining were used to assess mitophagy. The single-cell RNA sequencing (scRNA-seq) and bioinformatics analyses were used to detect transcription signature changes during aging.

Results. In this study, we discovered that aging increased oxidative stress, which increased apoptosis, and generated ROS in acinar epithelial cells. Furthermore, activation of PINK1/Parkin-mediated mitophagy by rapamycin reduced lacrimal gland ROS concentrations and prevented aging-induced apoptosis of acinar cells, thereby causing histological alterations, microstructural degradation, and increasing tear secretion associated with ROS accumulation. By contrast, Mdivi-1 aggregates mitochondrial function and thereafter leads to lacrimal gland function impairment by inhibiting mitochondrial fission and giving rise to mitophagy.

Conclusions. Overall, our findings suggested that aging could impair mitochondrial function of acinar cells, and age-related alterations may be treated with therapeutic approaches that enhance mitophagy while maintaining mitochondrial function.

Keywords: aged, mitophagy, lacrimal gland acinar cells, mitochondria, rapamycin

The biological process of aging is universal and leads to a wide range of gradual declines in physiological functions and tissue structure.[1] By 2050, the elderly population (60 years of age or over) around the world will reach 2 billion, and with the increase in human life expectancy and the growing global population aging, the incidence of aging-related ocular diseases is gradually increasing.[1,2] The changing demographics provide several healthcare and social issues. The available data indicate that many age-related disorders can be prevented or treated more slowly by regulating the biological mechanisms associated with aging.[3] Thus, it is critical to investigate the causes behind the progression of aging and the disorders that are related to it.

Dry eye disease (DED) is one of the most common ocular surface diseases affecting the quality of life of the elderly population, and aging is also one of the independent risk factors for DED.[2,4–6] According to epidemiological reports, the global prevalence of DED has reached 30% in people over 50 years of age.[7] According to epidemiological surveys, the prevalence of DED in China is 21% to 30% and the prevalence increases with age.[8] The socioeconomic impact of DED is significant, and the burden of disease it causes is becoming increasingly apparent. In the United States, total social expenditures related to DED are estimated to exceed $55 billion per year.[9]

The lacrimal gland is an exocrine gland that contributes mainly to the aqueous component of the tear film, and its

secretion constitutes the majority of the tear film (98% to 99%).[10] It consists of three main cell types: acinar epithelial cells, ductal epithelial cells, and myoepithelial cells. The most abundant type (about 80%), the acinar epithelial cells are highly polarized epithelial cells responsible for the synthesis and secretion of aqueous fluid that are essential for the maintenance of homeostasis of the ocular surface, and visual function.[10] The lacrimal gland is highly susceptible to the effects of aging,[11,12] which manifests as structural and functional damage, with major pathological changes, including acinar epithelial cells atrophy, periductal fibrosis, and chronic inflammatory cells infiltration, as well as a decrease in the density of nerves driving lacrimal secretion, which ultimately leads to qualitative and quantitative abnormalities in lacrimal gland secretions.[11,13,14] According to a meta-analysis, the prevalence of DED elevates from 1.3% to 9.2% in the elderly population when compared to the younger population.[10] Aqueous-tear-deficient DED (ADDE), one of the main types of DED, occurs when the aqueous component of tears is reduced, and ADDE has a high prevalence in the elderly population.[15] Thus, improving the quality of life for the middle-aged population requires a comprehension of the process of lacrimal gland aging and its underlying processes.

Mitochondria provide essential energy and substrates for cellular metabolism and growth through the mitochondrial respiratory chain. However, mitochondrial abnormalities lead to reduced energy supply and increased release of mitochondrial reactive oxygen species (mtROS), and mtROS trigger oxidative damage to proteins and mitochondrial DNA (mtDNA) present in the mitochondria, eventually leading to disruption of mitochondrial homeostasis and the onset of cellular senescence.[16–18] Lipids and proteins are susceptible to oxidative stress, and oxidative stress by-products accumulate in tissues to form lipofuscin-like particles, which are considered to be one of the hallmarks of senescence and autophagy abnormalities, and accumulation of lipofuscin-like particles can be observed in senescent lacrimal gland tissues.[13] Ultrastructural studies of the lacrimal gland have also shown that the mitochondrial inner membrane area in the acinar epithelial cells of middle-aged rats is significantly reduced and the mitochondrial alterations can be mitigated by the use of antioxidants, however, most of the ultrastructural changes in the lacrimal acinar epithelial cells could not be reversed by drugs.[19] The self-degradative process of autophagy, also known as macroautophagy, is crucial for recycling and digesting different cytoplasmic contents that are damaged or middle-aged.[20,21] Mitophagy is an essential process that contributes to maintaining mitochondrial homeostasis by eliminating impaired or dysfunctional mitochondria followed by degradation through lysosomes.[22,23] The most commonly recognized mitophagy pathway is the PINK1/Parkin pathway.[24] Aging impairs cellular mitophagy, which leads to an accumulation of damaged mitochondria and cell dysfunction, both of which worsen or contribute to aging.[25,26] Thus, promoting PINK1/Parkin-dependent mitophagy might be a way to treat age-related lacrimal gland impairment.

Senescence is a condition of cells that emerges in response to growth impulses or stress.[23] It is characterized by a steady stop to growth, robustness against cellular death, and the release of chemicals into the extracellular environment.[27] Senescent cells stop growing, but they still secrete a complex mixture of substances identified as the senescence-associated secretory phenotype (SASP), which includes angiogenesis factors, proteases, and pro-inflammatory cytokines. These substances can alter tissue microenvironments, alter tissue structure and function, and cause chronic inflammation.[28,29] An experimental data study shows that SASP was elevated in the lacrimal gland of chronic graft-versus-host disease (cGVHD) mice compared with control mice.[30] Recent studies revealed promoting mitophagy in a PINK1-dependent manner prevents senescence and SASP.[31] Previous studies have shown that rapamycin, a blocker of the mechanistic target of rapamycin complex 1 (mTORC1) pathway blocker, can prevent cellular and organismal aging by inhibiting SASP.[32,33]

A systematic understanding of the lacrimal gland in the context of aging is still lacking, despite growing evidence of significant pathological changes in the lacrimal gland during aging. It is now possible to comprehensively investigate the complexity of human illnesses, including a variety of cell types, cellular heterogeneity, and pseudo-time analysis, due to the techniques of single-cell RNA sequencing (scRNA-seq). This study aimed to explore PINK1-Parkin-dependent mitophagy in middle-aged lacrimal glands. We also investigated whether rapamycin affected cellular senescence and mitophagy. The findings of this study establish a connection among mitophagy, senescence, and lacrimal gland damage.

Methods

Animals and Treatment

Male C57BL/6J mice (6 weeks old 18–22 g and 12 months old 30–40 g) were acquired from the Changsha Tianqin Biotechnology Co., Ltd. (Changsha, Hunan, China). A steady room temperature of 25°C and a relative humidity of 40% to 60% were maintained in the laboratory animal center. Every mouse was kept in an ordinary setting with a 12-hour light/dark cycle. All animal protocols were approved by the Animal Ethics Committee of Xiangya Hospital of Central South University, which were in accordance with the ARVO Statement for the Use of Animals in Ophthalmic and Vision Research. To enhance or inhibit mitophagy in mice lacrimal glands, we intraperitoneally injected 5 mg/kg of rapamycin (#HY-10219, MedChemExpression, Monmouth Junction, NJ, USA) in sterile saline with 2% dimethyl sulfoxide (DMSO) or 10 mg/kg of Mdivi-1 (#HY-15886, MedChemExpression, Monmouth Junction, NJ, USA) in sterile saline with 2% DMSO once daily for 1 month, following a week of adaptation. Rapamycin was dissolved in DMSO (50 mg/mL), and Mdivi-1was dissolved in DMSO (25 mg/mL) as the storage solution.

Tear Secretion Measurement

Before and after treatment, tear secretion was assessed through phenol red thread (Tianjin Jingming New Technology Development Co., Ltd. Tianjin, China). Without the ocular surface anesthesia, the phenol red thread was held by microtome tweezers and placed in the outer canthus of both eyes of the mice for 20 seconds, and the length of the part of the phenol red thread that was wetted to turn red was measured as an estimate of the tear volume (in millimeters). Each eye was measured three times and the average value was taken.

Investigative Ophthalmology & Visual Science

Hematoxylin and Eosin and Masson Staining

In brief, an incision was made anterior to the ear, and the extraorbital lacrimal gland was exposed and then excised. The extraorbital lacrimal gland tissue that had been fixed in 5% paraformaldehyde was cut into 5 µm thick slices using paraffin embedding. The 5 µm paraffin slices were deparaffinized, rehydrated, and stained according to the manufacturer's instructions using Masson's Staining Kit (#G1006; Servicebio, Wuhan, China) and hematoxylin and eosin (H&E) staining kit (#G1005; Servicebio, Wuhan, China). Using a light microscope, histological images were observed and recorded (Nikon Eclipse E100; Nikon, Tokyo, Japan).

Oil Red O Staining

The lacrimal gland tissue that had been fixed in 5% paraformaldehyde was cut into 5 µm thick slices using optimum cutting temperature (OCT) embedding agent. Frozen lacrimal gland sections stained with the Oil Red O staining kit (#G1015; Servicebio, Wuhan, China) and incubated at room temperature in the dark for 2 hours. Then, the samples were observed by a light microscope (Nikon Eclipse E100; Nikon, Tokyo, Japan).

Mitochondrial Membrane Potential

JC-1 staining kit (#C2003; Beyotime, Shanghai, China) was conducted to evaluate the levels of mitochondrial membrane potential in the lacrimal gland tissue. After washing with PBS thrice for 5 minutes each, the 5 µm lacrimal gland paraffin sections were incubated with JC-1 dye in the dark at 37°C for 15 minutes. After washing again, the sections were sealed and visualized using a fluorescence microscope (Nikon Eclipse C1; Nikon, Tokyo, Japan). JC-1 dye is a cationic dye that accumulates in the mitochondria depending on the potential, causing the fluorescence to change from green to red.

ROS Staining

To measure the amount of ROS in the lacrimal gland tissue, a ROS detection kit (#C0063; Beyotime, Shanghai, China) was used. The 5 µm paraffin slices of the lacrimal gland were utilized in vivo. Samples in the sections were incubated with ROS in the dark for 30 minutes at 37°C after being cleaned 3 times for 5 minutes each with phosphate buffer saline (PBS; pH = 7.2, #abs962, Absin, Shanghai, China). The paraffin slices were sealed and examined using a fluorescent microscope (Nikon Eclipse C1; Nikon, Tokyo, Japan) following another round of washing.

TUNEL Kit Identified Apoptosis

Tissue apoptosis was detected using the TUNEL cell apoptosis detection kit (#G1502; Servicebio, Wuhan, China). The 5 µm paraffin slices of lacrimal gland tissues were treated with TdT incubation buffer for 1 hour at 37°C in the dark. The anti-fade mounting media was used to encapsulate the nuclei after they had been dyed with DAPI solution for 8 minutes at room temperature. Images were examined using an Olympus fluorescence microscope (Nikon Eclipse C1; Nikon, Tokyo, Japan).

Immunohistochemical Staining

The lacrimal gland paraffin sections were dewaxed, rehydrated, blocked (with 5% BSA) and then treated with primary antibodies overnight at 4°C. The antigen repair procedure was performed using 0.1 M sodium citrate buffer at pH 6.0 and 90°C in a water bath, per the antibody instruction. Following a 1-hour incubation period at room temperature with the secondary antibody, the sections were nucleated, sealed, examined, DAB staining (#BDAA0192; Biodragon, Suzhou, China), and captured on the light microscope (Nikon Eclipse E100; Nikon, Tokyo, Japan). Primary antibodies used were IL-1β (1:200, Servicebio, GB11113), IL-6 (1:200, Servicebio, GB11117), PPARγ (1:500, Servicebio, GB12164), NADPH oxidase 4 (NOX4; 1:1000, Servicebio, GB11347), and 3-nitrotyrosine (3-NT; 1:1000, Servicebio, GB112528).

Immunofluorescence Staining

The lacrimal gland paraffin sections were prepared and dried in a thermostat at 45°C. Fresh dimethylbenzene was used to dewax the slices twice, for a total of 5 to 10 minutes each time. After 5 minutes of 100% ethyl alcohol fixation, the slices were left in 85% ethyl alcohol, 75% ethyl alcohol, and distilled water for an additional 5 minutes each. After being incubated with proteinase K without DNase for 15 to 30 minutes at 20 to 37°C, the sections were cleaned 3 times using PBS. After the slices had slightly dried, a histochemical pen was used to create a circle around the tissue. After applying autofluorescence quench for 5 minutes, the circle was washed with water for 10 minutes. The slices were stained with DAPI and counterstained to identify nuclei. There were three 5-minute PBS washes on the sections. After being slightly dried, the slices were sealed with an anti-fluorescence quencher and kept in a 4-degree dark section box. With the use of an Olympus fluorescence microscope (Nikon Eclipse C1; Nikon, Tokyo, Japan), the images were captured. The following primary antibodies were used: CD45 (1:1000, Servicebio, GB113886), Ki67 (1:1000, Servicebio, GB121141), TOMM20 (1:5000, Servicebio, GB111481), LAMP-1 (1:4000, Servicebio, GB112949), Parkin (1:2000, Servicebio, GB114834), LC3B (1:1000, Servicebio, GB113801), p62 (1:3000, Servicebio, GB11531), γH2AX (1:1000, Servicebio, BA3677), p63 (1:500, Servicebio, GB15900), NaK-ATPase (1:2000, Servicebio, GB11902), αSMA (1:500, Servicebio, GB12045), and AQP5 (1:5000, Servicebio, GB113318).

Western Blot Analysis

A combination solution consisting of 1% phenylmethylsulfonyl fluoride (PMSF) and RIPA lysis buffer was used to extract the total proteins from the lacrimal gland tissues. The assay kit for bicinchoninic acid (BCA; #P0012; Beyotime, Shanghai, China) was utilized to identify the concentration of total protein. Proteins (30 µg) were transferred to polyvinylidene difluoride (PVDF) membranes after being separated using 8% to 12% sodium dodecyl-sulfate polyacrylamide gel electrophoresis (SDS-PAGE). The primary antibody was incubated onto the PVDF membranes for an entire night at 4°C until it had been blocked with 5% fat-free milk for 1 hour at 37°C. After being washed in Tris-Buffered Saline and Tween 20 (TBST; #AIWB-008, Swiss Affinibody LifeScience AG, Wuhan, China), the PVDF

Investigative Ophthalmology & Visual Science

membranes were incubated for 1 hour at room temperature with the horseradish peroxidase (HRP)-conjugated anti-rabbit IgG antibody (1:10000; Servicebio, Wuhan, China). The enhanced chemiluminescence reagent (ECL) detection kit (#PD0001; CYTOCH, Shanghai, China) was used to identify the immune-labeled protein bands. The Imaging System (SCG-W2000; Servicebio, Wuhan, China) was used to capture the images, and Image J was used to quantify the results. The details of primary antibodies were shown in the following: p16 (1:3000, Proteintech, 10883-1-AP), p21 (1:4000, Proteintech, 10355-1-AP), LC3B (1:1000, ZENBIO, 381544), p62 (1:1000, ZENBIO, 380612), p-mTOR$^{(Ser2448)}$ (1:1000, Proteintech, 67778-1-Ig), mTOR (1:1000, Proteintech, 28273-1-AP), Beclin-1 (1:4000, Proteintech, 11306-1-AP), DRP1 (1:1000, Affinity Biosciences, DF7037), MFF (1:2000, Proteintech, 17090-1-AP), PINK1 (1:1000, Affinity Biosciences, DF7742), Parkin (1:1000, ZENBIO, 381626), and GAPDH (1:10000, Servicebio, GB15002).

Quantitative Real-Time PCR

Using a SteadyPure Quick RNA Extraction kit (#AG21023; Accurate Biotechnology [Hunan] Co., Ltd., Changsha, China) and the manufacturer's instructions, total RNA from lacrimal gland tissues was extracted. Following isolation, the reverse transcription premix kit (#AG11728; Accurate Biotechnology [Hunan] Co., Ltd., Changsha, China) was used to synthesize cDNA and assess the amount of RNA. The real-time PCR was performed using the SYBR Green qPCR Kit (#AG11701; Accurate Biotechnology [Hunan] Co., Ltd., Changsha, China). The comparative Ct technique was used to examine the quantitative PCR data, and the findings were standardized to the Ct value of GAPDH. The primers used are listed in Supplementary Table S1.

mtDNA Measurement

Using the Steadypure universal genomic DNA extraction kit (#AG21009; Accurate Biotechnology [Hunan] Co., Ltd., Changsha, China), total DNA from lacrimal gland tissue was extracted. mtDNA was then amplified with COX2 gene primers using real-time PCR and normalized to ribosomal gene Actin. The primers used are listed in Supplementary Table S2.

Transmission Electron Microscope

The lacrimal gland tissues were treated using 1% OsO_4 and 3% glutaraldehyde. The samples were placed in acetone for 20 minutes of incubation after being dehydrated for 15 to 20 minutes in a graded series of ethanol solutions (30%-50%-70%-80%-95%-100%-100%). An ultrathin section of 60 to 80 nm was inserted into the copper mesh. It was stained for 10 to 15 minutes at room temperature with uranium acetate, and then for 1 to 2 minutes with lead citrate. Finally, the Hitachi Transmission Electron Microscope (TEM) system (HT7800; Hitachi, Tokyo, Japan) was used for observing ultrathin sections and taking images.

Mice Lacrimal Gland Digestion

Under the operating microscope, fresh extraorbital lacrimal glands from young mice ($N = 3$) and middle-aged mice ($N = 3$) were quickly separated, and they were then stored in the sterile, ice-cold Tissue Preservation Solution buffer. The samples were digested using 2 to 3 mL of trypsin solution (#C3538; VivaCell, Shanghai, China) at 37°C after being washed with Hanks' Balanced Salt (#211031; NEST Biotechnology, Wuxi, China). For 15 minutes, gentle pipetting was used to break down the tissue until no visible blockage was observed. The mixture was then centrifuged at 350 × g for 5 minutes, and PBS was used to gently resuspend it. Finally, trypan blue (Beyotime, Shanghai, China) was used to stain the samples, and Countess II Automated Cell Counter (Thermo Fisher Scientific, Fair Lawn, NJ, USA) was used to determine the cell viability.

Processing of scRNA-seq

After tissue digestion, single-cell suspensions (1×10^5 cells/mL) were placed into microfluidic devices, and the 10× Genomics (Pleasanton, CA, USA) chromium platform was used to process the scRNA-seq data. RNA was liberated and reverse-transcribed into cDNA following lysing, marking with a unique molecular identifier (UMI), and being barcoded. The processed cDNA was then used to build the scRNA-seq libraries. High-throughput sequencing of constructed libraries using the Illumina sequencing platform in double-ended sequencing mode.

Quality Control and Analysis of scRNA-seq Data

An internal workflow was used to process the raw data and provide gene expression profiles. The number of UMI of genes in each cell was determined by grouping readings based on the barcode, UMI, and gene. For further research, each cellular barcode's UMI count tables were used. Cell Ranger (10× Genomics, Pleasanton, CA, USA) and the Seurat R package (version 4.0.0) were used for quality control and raw data preparation. We further filtered the cells using several metrics to retain high-quality cells. These metrics include (i) the number of genes identified in a single cell (200–8000); (ii) the total number of UMIs in single cells less than 50,000; and (iii) mitochondrial reads less than 25%. After retaining high-quality cells, we homogenized the expression using log homogenization. We used Harmony R package for data merging and batch effect correction. Seurat R package (version 4.1.0) was used to cluster cells. Afterward, we used the rank sum test in the Seurat R package (version 4.1.0) for differentially expressed gene (DEG) analysis of different cell subpopulations to screen for genes upregulated for expression in each cell subpopulation with the standard of $|\log2 \text{(fold change)}| > 0.5$ and $P < 0.05$. Moreover, the gene collection was subjected to pseudo-time analyses using Monocle2 (version 2.26.0), Gene Ontology (GO), Kyoto Encyclopedia of Genes and Genomes (KEGG), and REACTOME function enrichment analysis using the clusterProfiler (version 4.6.2). The volcano plot and heatmap functions were used to visualize the findings of scRNA-seq analysis. Mitophagy-related genes (MRGs) were downloaded from "RECTOME-MITOPHAGY. Mms". The fgsea R package was used to perform Gene Set Enrichment Analysis (GSEA). The Mococle2 R package was used for the analysis of pseudotime analysis in order to measure the dynamics of cells during development, differentiation, and senescence.

Statistical Analysis

The statistical analysis was carried out using GraphPad Prism version 9.0.0 (GraphPad, La Jolla, CA, USA). Results of the study were evaluated using the Student's *t*-test or 1-way analysis of variance, and the results are displayed as the

mean ± SEM. There was a statistically significant difference between the 2 groups when the P value was less than 0.05.

Results

The Age-Related Histological and Functional Alterations in Mice Lacrimal Gland Acinar

Histological staining was conducted on lacrimal gland samples from both younger and middle-aged mice. When comparing middle-aged lacrimal glands to younger ones, H&E staining revealed a decrease in the number of acinar tissue, heterogeneity in the size, disorganized arrangement and polar orientation, and an increased karyoplasmic ratio (Fig. 1A). We then studied lipid deposition in middle-aged lacrimal glands, as lipid dysregulation is commonly associated with aging.[34] Neutral triglycerides and lipids will be stained by Oil red O staining and used to identify sections of young and middle-aged lacrimal glands. Lipid droplets in young lacrimal glands are tiny intracellular lipid droplets. By contrast, lipid droplets gathered together to form bigger structures in middle-aged lacrimal gland. The greater visibility of these bigger structures was observed among acinar cells, inside ducts, and at the border of immune cell infiltrates (Fig. 1B). Through Masson staining, collagen appears blue in bright-field imaging. As a result, regions of the accumulation of collagen were observed by Masson staining, and this was higher in the middle-aged extracellular matrix (ECM) in the lacrimal gland than those in the young group ($P < 0.001$; Figs. 1C, 1D). Cells positive for immune cell marker CD45 were also present and were consistently located in the outer layer of acini and ducts ($P < 0.001$; Fig. 1E). Of note, we found that the percentage of ki67-positive cells was approximately 15% higher in the young lacrimal gland compared to the middle-aged group ($P < 0.001$; Fig. 1F). TUNEL-positive cells gradually increased in the lacrimal gland of middle-aged mice (Supplementary Fig. S1A). Moreover, γH2AX-positive cells were significantly increased and distributed in the acinar cells of middle-aged mice (Supplementary Fig. S1B). To investigate the level of lipid metabolism gene (PPARγ) and SASP factors, we first examined protein levels of IL-1β, IL-6, and PPARγ. Immunohistochemical (IHC) analyses showed a significant increase in IL-1β, IL-6, and PPARγ expression in the middle-aged lacrimal gland compared to the young lacrimal gland ($P < 0.001$; Fig. 1G). In addition, lipid-metabolism-related markers, carnitine palmitoyltransferase 1a (CPT1a), carnitine palmitoyltransferase 2 (CPT2), and C/EBPα, were upregulated in the middle-aged mice group ($P < 0.001$; Fig. 1H). Western blot results showed that expression levels of P16 and p21 increased significantly in the middle-aged lacrimal gland compared to the young lacrimal gland ($P < 0.01$; Figs. 1I, 1J). The tear secretion was lower in the middle-aged mice than in the young mice ($P < 0.001$; Fig. 1K).

Aging Caused ROS Generation and Mitochondrial Dysfunction in Mice Lacrimal Gland Acinar

To investigate age-related changes in oxidative stress in the lacrimal gland, we measured ROS levels using ROS dye staining in young and middle-aged mice. Our findings demonstrated a significant rise in ROS levels in the lacrimal gland of middle-aged mice in contrast to young ones ($P < 0.001$; Figs. 2A, 2B). We also found that mtDNA leakage was upregulated in the middle-aged mice group ($P < 0.001$; Fig. 2C). ROS are mostly produced by mitochondria, which are also the site of cellular energy metabolism. We next used a fluorescent probe, JC-1 dye, to detect the mitochondria membrane potential in lacrimal gland acinar cells. The JC-1 result demonstrated a reduction in the potential of the mitochondrial membrane in middle-aged mice, which suggested mitochondrial injury ($P < 0.001$; Figs. 2D, 2E). The immunofluorescence staining analysis revealed that the immunofluorescence intensity of mitochondria decreased in the lacrimal gland (Fig. 2F). According to the LAMP-1 Red fluorescent data, there was a noticeable lysosomal production in the middle-aged lacrimal gland (Fig. 2G). A TEM was used to observe the effects of the age-related mitochondrial alterations. In middle-aged lacrimal glands, the mitochondrial area and perimeter are significantly reduced ($P < 0.001$; Figs. 2H, 2I). Following aging, a small number of mitochondrial hypermegasoma emerged, indicating aberrant mitochondrial metabolism. Moreover, we noticed that the lipid droplets had significantly decreased and that the lipid droplets had eventually amalgamated into larger ones in the middle-aged lacrimal gland ($P < 0.001$; Figs. 2J, 2K). Our findings demonstrated that aging caused an increase in cellular ROS, which were detected using the ROS fluorescent probe. When total ROS was stained with ROS dye, red fluorescence significantly increased. The ultrastructure of mitochondria was also significantly altered. These findings imply that aging caused ROS levels to rise and mitochondrial malfunction.

PINK1/Parkin-Mediated Mitophagy is Associated With Lacrimal Gland Acinar Function During the Aging Process

To determine the mechanism for aging impact on lacrimal gland acinar function, we deeply investigated transcription signatures that occurred in the lacrimal gland by 10× Genomics-based scRNA-seq (Fig. 3A). Twelve cell types were identified in the lacrimal gland based on their specific transcriptional profiles (Figs. 3B–E)[35–38]: acinar epithelial cells (*Bhlha15*, *Scgb2a2*, *Lpo*, *Aqp5*, and *Pip*), ductal epithelial cells (*Sftpd*, *Wfdc2*, *Anxa1*, and *Slc1a2*), myoepithelial cells (*Acta2*, *Cnn1*, *Actg2*, *Krt5*, *Krt14*, and *Krt17*), mesenchymal cells (*Dcn*, *Lum*, and *Gsn*), fibroblasts (*Col1a1*, *Col1a2*, and *Col3a1*), smooth muscle cells (*Acta2*, *Tagln*, *Myh11*, and *Actg2*), endothelial cells (*Kdr*, *Cdh5*, and *Pecam1*), T cells (*Cd3e*, *Cd3g*, *Cd3d*, *Cd8a*, *Ccl5*, and *Lef1*), B cells (*Cd79a*, *Cd79b*, *Cd19*, and *Cxcr5*), macrophage cells (*Cd68*, *Cd168*, *C1qa*, *Adgre1*, *Mrc1*, and *Fcgr1*), plasma cells (Mzb1, Ighg1, Igkc, Ighg3, Xbp1, and Jchain), and dendritic cells (DCs; *Cst3*, *Irf8*, *Siglech*, *Ccr9*, and *Cd209a*).

We observed a dramatically decreased percentage of acinar epithelial cells in middle-aged lacrimal glands compared to young lacrimal glands. On the other hand, the percentage of immune cells in middle-aged lacrimal glands considerably increased. Furthermore, the percentage of myoepithelial cells in the middle-aged lacrimal gland was drastically decreased. Compared to the aforementioned populations, there was a small reduction in the makeup of ductal cells. T cells increased significantly in the middle-aged lacrimal gland within the immune cells compartment, whereas the percentage of macrophages/monocytes increased moderately and the percentage of NK cells and B cells was similar. Regarding stromal cells, fibroblasts

Investigative Ophthalmology & Visual Science

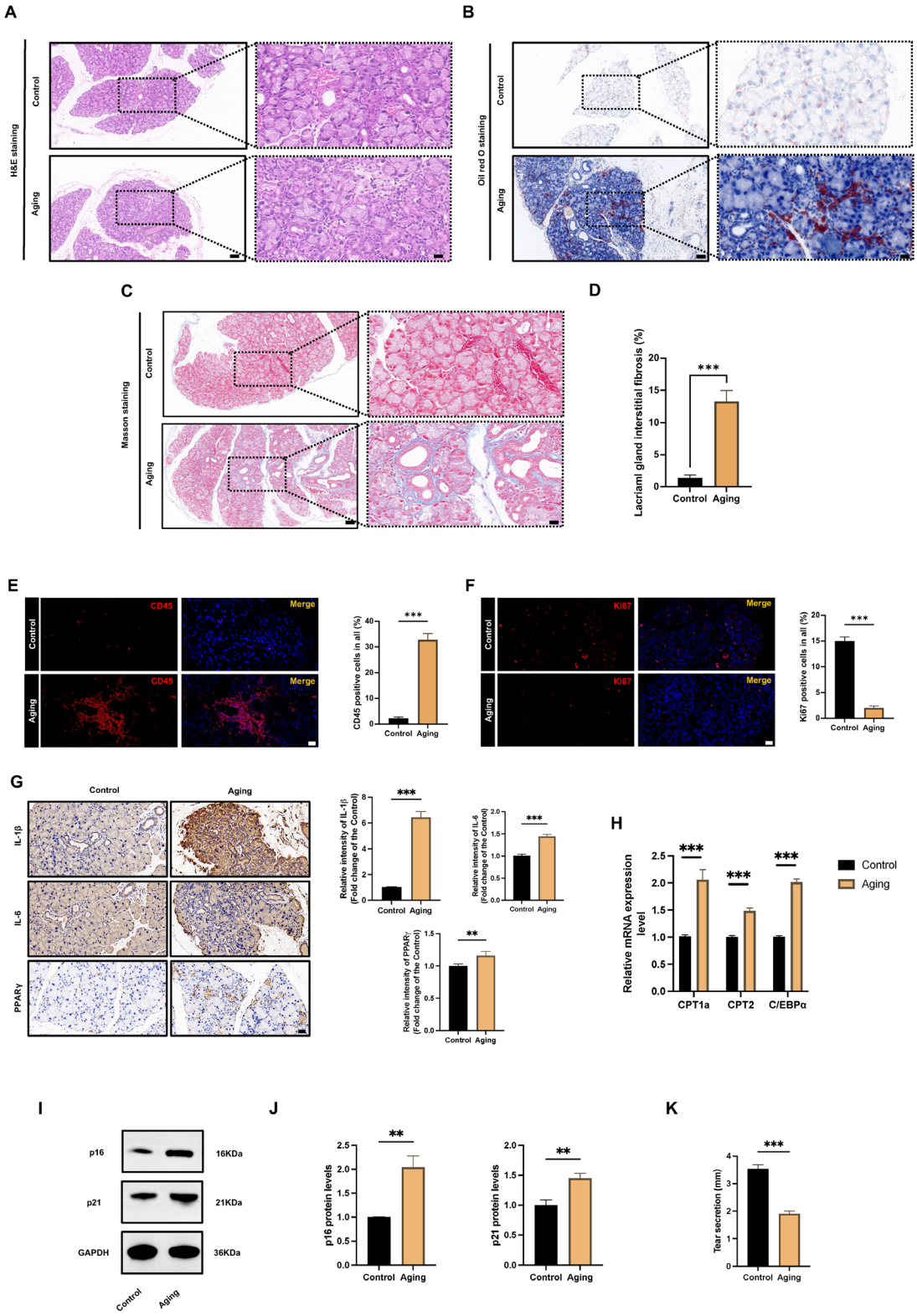

Figure 1. Morphological and histological assessment of control and middle-aged lacrimal gland. (**A**) Representative images of hematoxylin and eosin (H&E) staining in the lacrimal gland of control and middle-aged mice. (**B**) Representative macroscopic images of Masson staining in the lacrimal gland of control and middle-aged mice. (**C**) Oil Red O staining shows the lipid droplets in the lacrimal gland of control and middle-aged mice. (**D**) Quantitative analysis of the lacrimal gland interstitial fibrosis. (**E**) Immunofluorescent staining and quantifications of CD45 show immune cell infiltration in the lacrimal gland in control and middle-aged mice. (**F**) Immunofluorescent staining and quantifications of Ki67 show proliferative cell infiltration in the lacrimal gland in control and middle-aged mice. (**G**) Representative microscopic images of immunohistochemistry (IHC) of IL-1β, IL-6, and PPARγ expressions in the lacrimal gland of control and middle-aged mice. (**H**) The relative mRNA expression of CPT1a, CPT2, and C/EBPα in the lacrimal gland in control and middle-aged mice. (**I**) Western blot analysis showed the expression of p16 and p21 in lacrimal gland tissues. (**J**) Quantitative analysis of the levels of p16 and p21. (**K**) Tear secretion of each group of mice via phenol red thread test. Scale bar = 50 µm (magnified 20 µm) (**A**, **B**, **C**), 20 µm (**E**, **F**, **G**), $N = 4$, $^{**}P < 0.01$, $^{***}P < 0.001$.

Investigative Ophthalmology & Visual Science

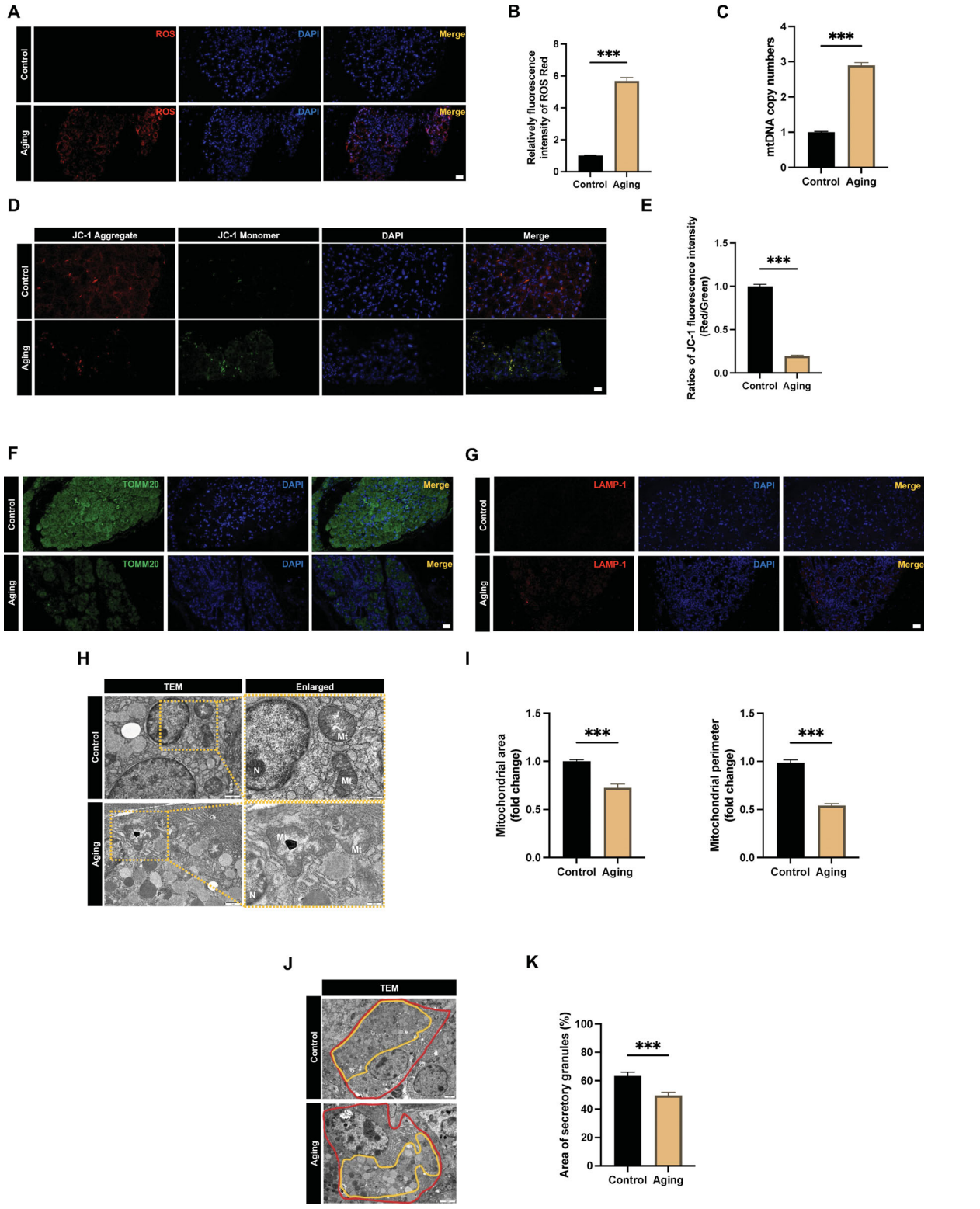

Figure 2. Reactive oxygen species (ROS) accumulation and mitochondrial dysfunction of the lacrimal gland in middle-aged mice. (**A**) Immunofluorescence staining of ROS using ROS probe (*red*) and DAPI (*blue*) in lacrimal gland tissues of control and middle-aged mice. (**B**) Assessment of relative fluorescence intensity of ROS staining. (**C**) Mitochondrial DNA (mtDNA) leakage in the lacrimal gland tissues in the different groups. (**D**) Immunofluorescence staining of mitochondrial membrane potential using JC-1 in lacrimal gland tissues of control and middle-aged mice. (**E**) Measurement of relative fluorescence intensity of JC-1 staining. (**F**) Representative immunofluorescence images for detecting TOMM20 (*green*) and DAPI (*blue*) of the lacrimal gland. (**G**) Representative immunofluorescence images for detecting LAMP-1 (*red*) and DAPI (*blue*) of the lacrimal gland. (**H**) Transmission electron microscopy (TEM) images of the ultrastructure of the acinar cells of the lacrimal gland in each group of mice. N, nucleus, Mt, mitochondria. (**I**) Measurement of mitochondrial area and perimeter on the TEM images. (**J**) TEM images of the ultrastructure of the secretory granules in the acinar cells of the lacrimal gland in control and middle-aged lacrimal glands. (**K**) Measurement of secretory granules (marked *yellow*) of acinar cells (marked *red*) on the TEM images. Scale bar = 20 µm (**A**, **D**, **F**, **G**), 1 µm (magnified 500 nm) (**H**, **J**), $N = 4$, ***$P < 0.001$.

Investigative Ophthalmology & Visual Science

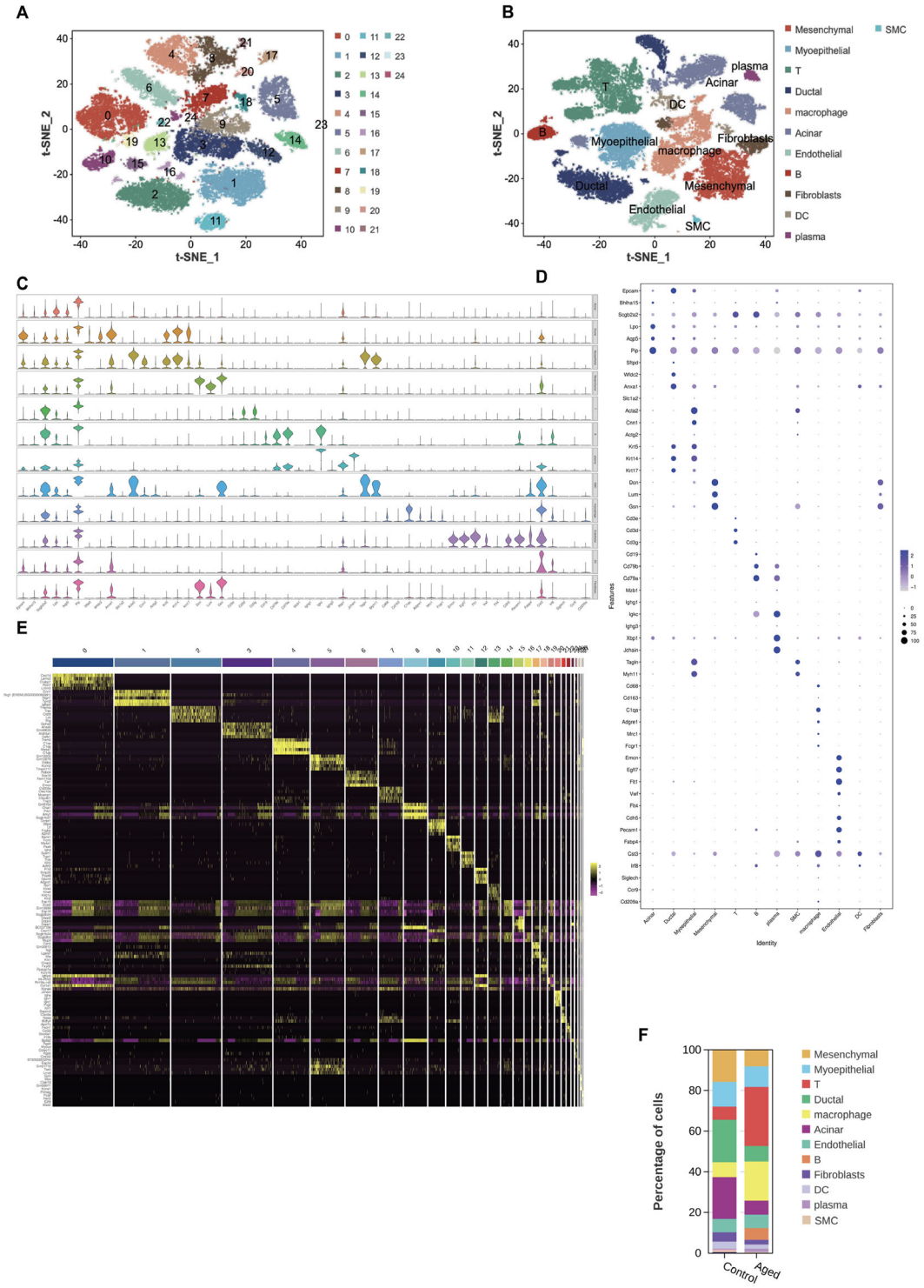

Figure 3. Single-cell transcriptomes atlas of the lacrimal gland of control and middle-aged mice. (**A**) The t-SNE plot showed individual cells colored by 25 cellular clusters. (**B**) The t-SNE plot showed the 12 cell types by identified by different cell markers. (**C**) The bar plot showed the cell proportions of the 12 cell clusters. (**D**) Violin plots of the expression of the marker gene in the 12 cell clusters. (**E**) Bubble plots of the expression of marker gene in the 12 cell clusters. (**F**) The heatmap showed the expression signatures of the top 100 DEGs that are expressed differently across each kind of cell. DEGs, differentially expressed genes.

contributed little to the middle-aged lacrimal gland, whereas the percentage of endothelial decreased (Fig. 3F).

The majority of the mouse lacrimal gland is made up of acinar epithelial cells, which are epithelial cells with the most severely altered gene expression. We isolated acinar epithelial cells and further divided them into seven subgroups (Fig. 4A). In middle-aged lacrimal gland acinar cells, DEG analysis revealed upregulated genes and downregulated genes (Figs. 4B, 4C). Based on these DEGs, GO enrichment analysis and KEGG, respectively, were performed. Mitophagy was the important functional cluster containing upregulated gene terms. The expression of mitophagy-related genes in the PINK1/Parkin-mediated mitophagy pathway was increased in acinar epithelial cells. In addition, lacrimal gland acinar cells from middle-aged mice exhibited mitophagy, as evidenced by significant degradation of the mitochondrial outer membrane protein TOMM20 (Figs. 4D–G). Collectively, this suggests that aging could promote mitophagy in acinar epithelial cells.

In order to explore the relationship between MRGs and DEGs of acinar epithelial cell clusters, we intersected 30 MRGs with 3744 DEGs (Supplementary Table S3). Fourteen differentially expressed MRGs (DE-MRGs) were found, including Ubc, Prkn, Sqstm1, Csnk2a1, Mfn1, Ubb, Csnk2a2, Atg5, Tomm20, Pink1, Tomm7, Tomm5, Ulk1, and Tomm22 (Fig. 5A). Each differentially expressed MRGs were plotted on a heatmap and bubbles plot (Figs. 5B, 5C). In diverse cell clusters, Ubc, Sqstm1, Ubb, Tomm7, Tomm20, Csnk2a2, Csnk2a1, and Tomm22 were extensively dispersed. Whereas acinar epithelial cells exhibited a relative overexpression of Prkn, Mfn1, and Pink1. The ductal cells expressed Ulk1 (Fig. 5D). Subsequently, we analyzed the expression of 14 DE-MRGs in different acinar epithelial cell subsets. The results indicated that Csnk2a1, Mfn1, Ubb, Csnk2a2, Atg5, Pink1, Tomm7, and Tomm5 were widely distributed in all kinds of acinar epithelial cells. Notably, Ubc, Sqstm1, and Ubb were highly expressed in 0 and 4 clusters. Ulk and Tomm22 were highly expressed in 4 clusters (Fig. 5E). We analyzed the cell trajectory differentiation of each epithelial cell using Monocle2. Different colors were assigned to each of the seven differentiated states, as seen in Figure 5F. The subclusters and aged distribution of acinar epithelial cells were mostly identified (Figs. 5G, 5H). The expression of 18 DE-MRGs changed with different differentiation states (Fig. 5J). It is noticeable that acinar epithelial cells differentiate from left to right throughout time—the deeper the blue, the more rapidly the differentiation (Fig. 5I).

Rapamycin Reverses Age-Induced Histological and Functional Alterations in the Lacrimal Gland

To assess the impact of rapamycin on lacrimal gland structure and function, rapamycin was applied to middle-aged mice. As a result, the mice were given the rapamycin (5 mg/kg). The results of H&E and Oil red O staining suggested that the acinar cells of the lacrimal gland showed normal organization and intracellular lipid accumulation was reduced after administration of rapamycin as compared to the middle-aged mice group (Figs. 6A, 6B). Notably, the administration of rapamycin alleviated the accumulation of collagen caused by aging ($P < 0.001$; Figs. 6C, 6D). Immunofluorescence staining for CD45 also showed that the lacrimal gland revealed a broad distribution of inflammatory cell infiltration in the periacinar, periductal, and interstitial of mice in the middle-aged group, rapamycin treatment markedly decreased the inflammatory cell infiltration (Fig. 6E). TUNEL-positive cells gradually decreased in the lacrimal gland of middle-aged mice treated with rapamycin (Supplementary Fig. S2A). In addition, we also found that treatment with rapamycin significantly increased the level of proliferation in the acinar cells in the lacrimal gland of the middle-aged mice (Fig. 6F). To further determine the anti-SASP effect of rapamycin treatment, we observed the expression of IL-1β and IL-6 throughout the lacrimal gland of mice by using the IHC staining. IL-1β and IL-6 in the middle-aged mice group were significantly higher compared with the young group, rapamycin intervention reduced the expression of SASP ($P < 0.001$; Fig. 6G). Based on quantitative real-time PCR, rapamycin-treated aged mice showed lower relative mRNA expression of CPT1a, CPT2, and C/EBPα in the lacrimal gland than aged mice (Fig. 6H). Their tear secretion increased due to this treatment than in the aged mice ($P < 0.01$ and $P < 0.001$; Fig. 6I). Together, these results demonstrated that the age-induced lacrimal gland acinar injury can be attenuated by rapamycin treatment in mice.

Rapamycin Alleviates Oxidative Stress and Mitochondrial Damage in the Lacrimal Gland of Mice

Mitochondrial damage and excessive generation of oxidative stress play crucial roles in mice lacrimal gland aging. To assess the generation of ROS in the lacrimal gland, we examined ROS levels. We observed an increase in levels of ROS in the lacrimal gland of the middle-aged mice group, which was significantly downregulated under rapamycin treatment ($P < 0.001$; Figs. 7A, 7B). We found that mtDNA leakage was downregulated in the rapamycin group ($P < 0.001$; Fig. 7C). Moreover, γH2AX-positive cells were significantly downregulated in the acinar cell of middle-aged mice treated with rapamycin (see Supplementary Fig. S2B). The JC-1 results indicated a reduction in the mitochondrial transmembrane potential of the lacrimal gland of the middle-aged mice group. However, rapamycin therapy has the ability to reverse the decrease in mitochondrial membrane potential, as indicated by a more significant change in fluorescence from green to red, indicating an apparent increase ($P < 0.001$; Figs. 7D, 7E). In the next study, to investigate the changes in the oxidative stress marker expression more closely, we performed the IHC assay in the lacrimal gland. Compared to the control group, acinar epithelial cells displayed higher expression of NOX4 (a major source of ROS) and 3-NT (a peroxynitrite stress marker). In contrast, these effects were partially reversed by rapamycin treatment. Compared with the control group, the levels of p-mTOR$^{(Ser2448)}$ of middle-aged mice in the rapamycin treatment model group were increased ($P < 0.05$ and $P < 0.001$; Fig. 7F). To further explore the mechanism of lacrimal gland acinar epithelial cells mitophagy in middle-aged mice, we detected the levels of the mammalian target of rapamycin (mTOR) pathway. The results showed that rapamycin markedly upregulated the levels of p-mTOR$^{(Ser2448)}$ ($P < 0.05$; Figs. 7G, 7H). These results suggested that rapamycin treatment reduces excessive ROS and restores mitochondrial function.

Investigative Ophthalmology & Visual Science

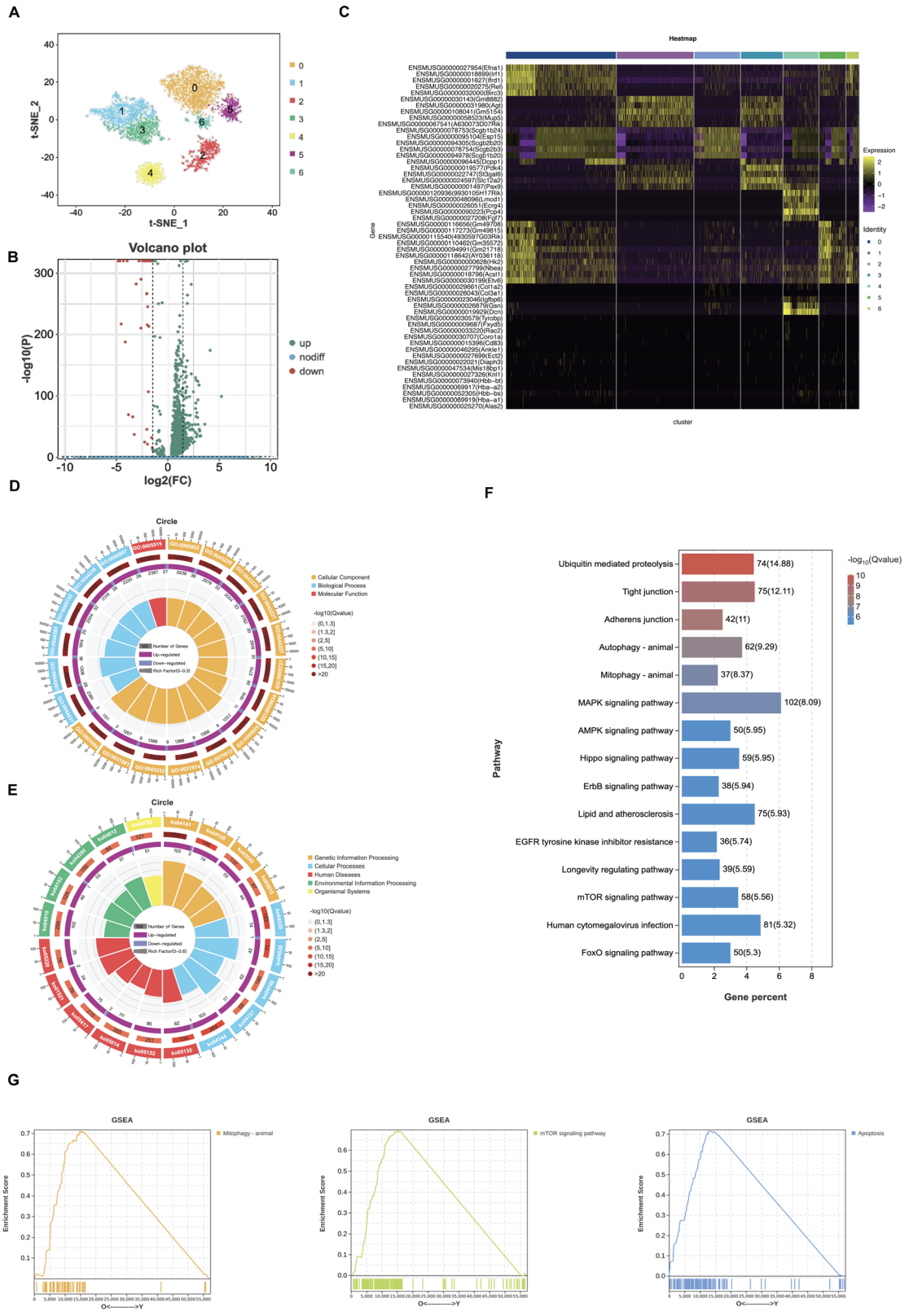

Figure 4. Analysis of mice lacrimal gland acinar epithelial cell subclusters. (**A**) The t-SNE plot showed reclustered epithelial cells, colored by clusters. (**B**) Volcanic map for DEGs of lacrimal gland acinar epithelial cell between control and aged group. (**C**) The heatmap showed the expression signatures of the top 50 DEGs that are expressed differently across each kind of subcluster. (**D**) GO analysis of DEGs. (**E**) KEGG analysis of DEGs. (**F**) The bar plot for 15 pathways is based on transcriptome sequencing results. DEGs, differentially expressed genes. (**G**) GSEA analysis of mitophagy pathway, mTOR pathway, and apoptosis pathway between control and aged group. DEGs, differentially expressed genes; GSEA, Gene Set Enrichment Analysis.

Investigative Ophthalmology & Visual Science

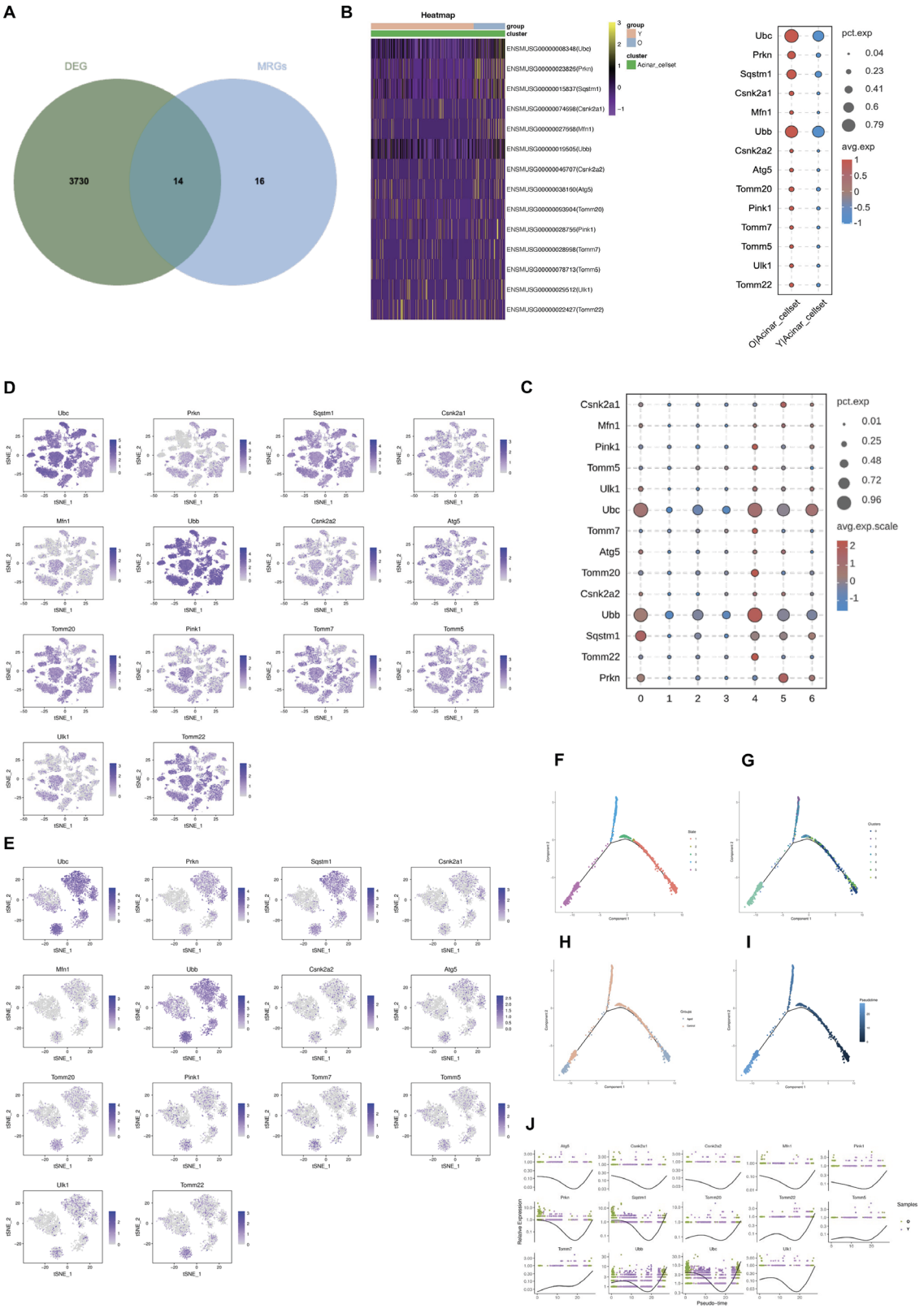

Figure 5. The mitophagy pathway during aging in mice lacrimal gland acinar epithelial cell subclusters. (**A**) The Venn plot displayed the overlapping genes between DEGs of lacrimal gland acinar epithelial cells between the control and aged group and MRGs. (**B**) The heatmap and bubble plots showed the distribution of DE-MRGs between the control and aged groups. (**C**) The bubble plots showed the distribution of DE-MRGs across the lacrimal gland acinar cell subclusters. (**D**) The t-SNE plot showed the DE-MRGs in lacrimal gland clusters. (**E**) The t-SNE plot showed the DE-MRGs in each lacrimal gland acinar epithelial cell subcluster. Differentiation trajectory of lacrimal gland acinar epithelial cell, colored for state (**F**), cell types (**G**), age distribution (**H**), and pseudo-time (**I**). (**J**) The differentiation pseudo-time trajectory of 14 DE-MRGs and their respective expression patterns. MRGs, mitophagy-related genes; DE-MRGs, differentially expressed mitophagy-related genes.

Investigative Ophthalmology & Visual Science

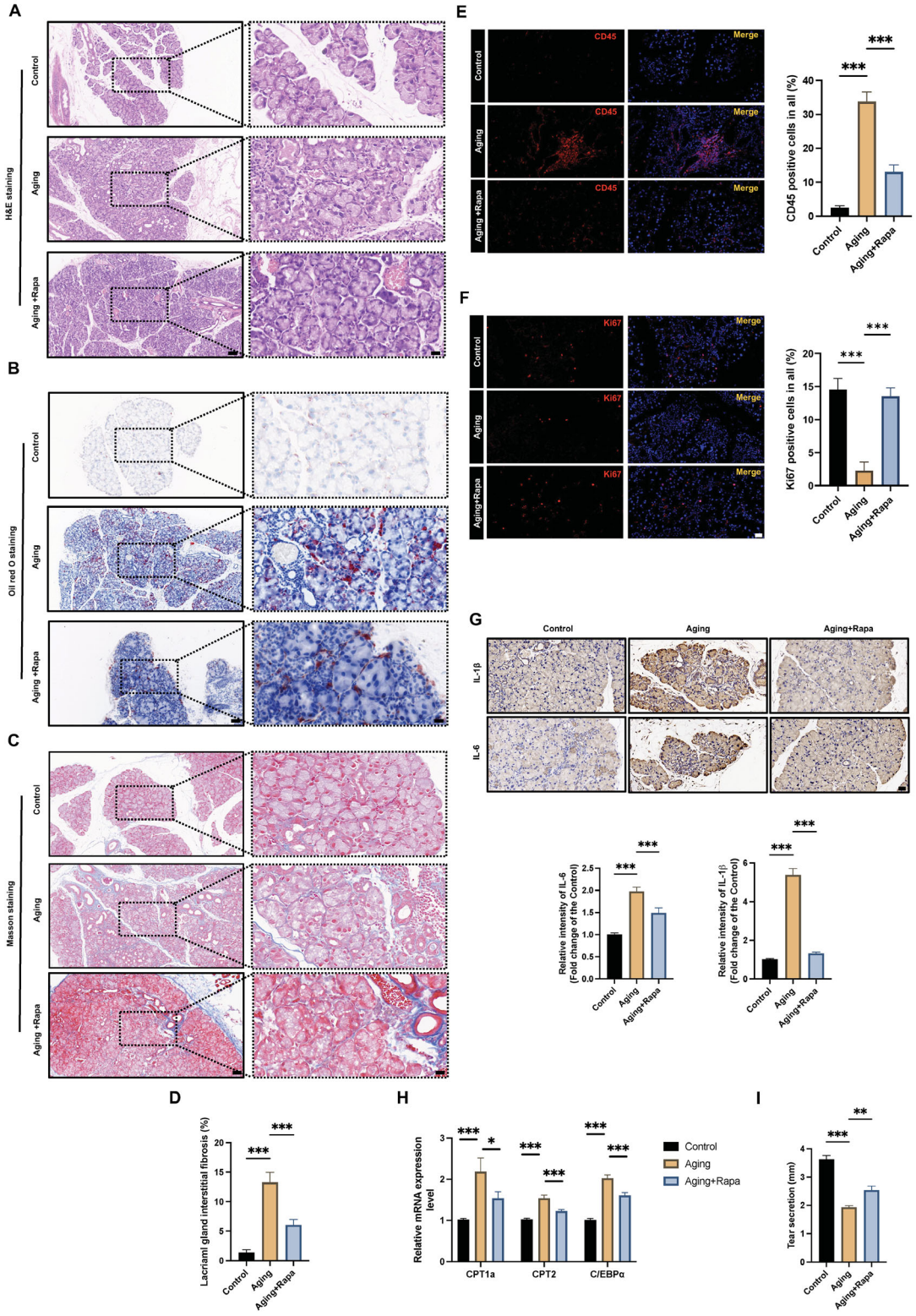

Figure 6. Rapamycin ameliorates morphological and histological damage of lacrimal gland acinar cells of middle-aged mice. (**A**) Representative images of hematoxylin and eosin (H&E) staining in the lacrimal gland of each group of mice. (**B**) Representative macroscopic images of Oil Red O staining in the lacrimal gland of each group of mice. (**C**) Masson staining shows the lipid droplets in the lacrimal gland of each group of mice. (**D**) Quantitative analysis of the lacrimal gland interstitial fibrosis. (**E**) Immunofluorescent staining and quantifications of CD45 show $CD45^{+}$ cell infiltration in the lacrimal gland of each group of mice. (**F**) Immunofluorescent staining and quantifications of Ki67 show $Ki67^{+}$ cells infiltration in the lacrimal gland of each group of mice. (**G**) Representative microscopic images of immunohistochemistry (IHC) of IL-1β and IL-6 expressions in mice control and middle-aged lacrimal gland. (**H**) The relative mRNA expression of CPT1a, CPT2, and C/EBPα in the lacrimal gland of each group of mice. (**I**) Tear secretion of each group of mice. Scale bar = 50 µm (magnified 20 µm) (**A**, **B**, **C**), 20 µm (**E**, **F**, **G**), $N = 4$, $^{**}P < 0.01$, $^{***}P < 0.001$. Rapa, rapamycin.

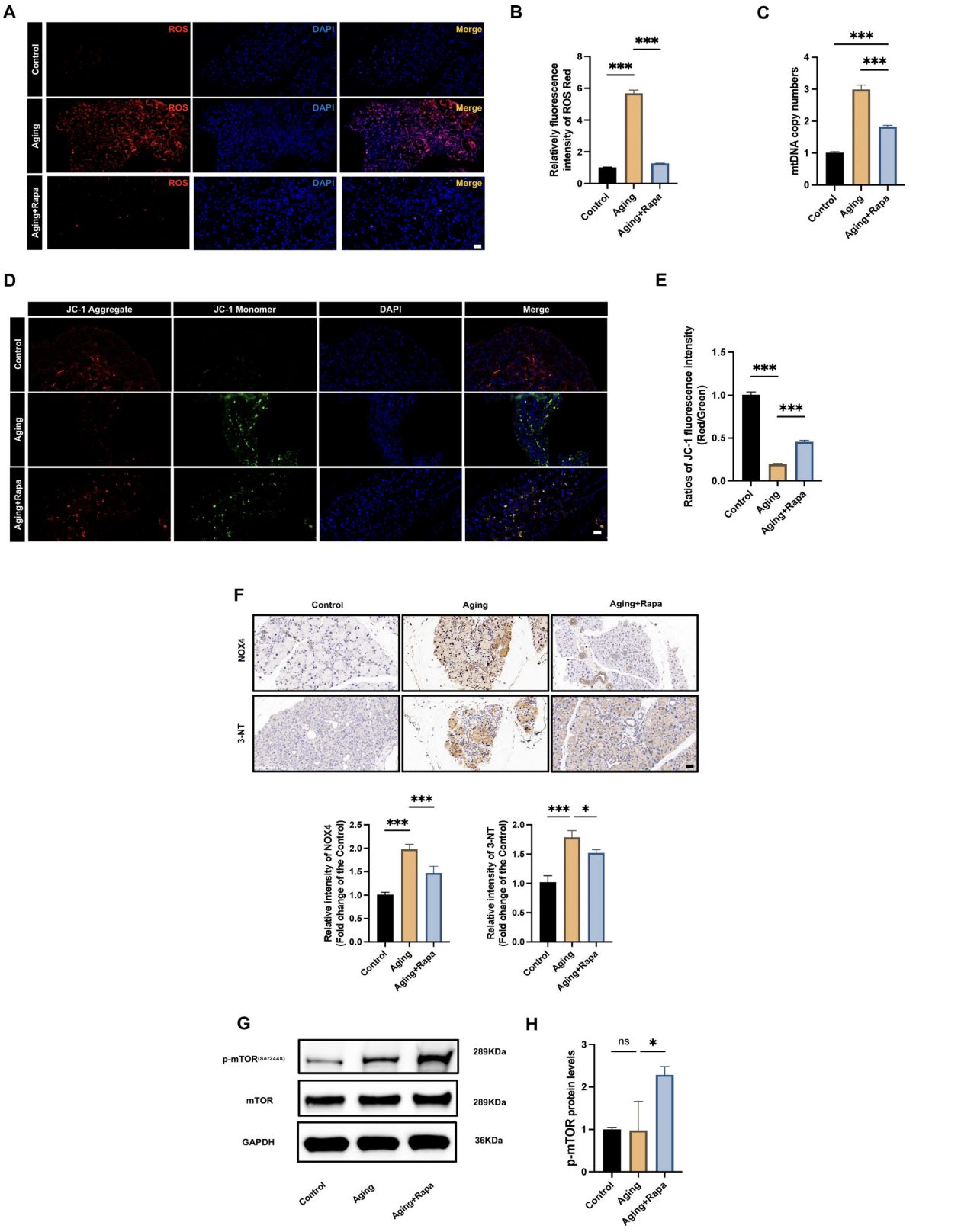

Figure 7. Rapamycin reverses aging-induced reduction in ROS production mitochondrial membrane potential and mitochondrial dysfunction. (**A**) Immunofluorescence staining of ROS using ROS probe (*red*) and DAPI (*blue*) in lacrimal gland tissues of each group of mice. (**B**) Assessment of relative fluorescence intensity of ROS staining. (**C**) Mitochondrial DNA (mtDNA) leakage in the lacrimal gland tissues in the different groups. (**D**) Immunofluorescence staining of mitochondrial membrane potential using JC-1 in lacrimal gland tissues of each group of mice. (**E**) Measurement of relative fluorescence intensity of JC-1 staining. (**F**) Representative microscopic images of immunohistochemistry (IHC) of NOX4 and 3-NT expressions in mice control and middle-aged lacrimal gland. (**G**) Western blot analysis showed the expression of p-mTOR$^{(Ser2448)}$ in lacrimal gland tissues. (**H**) Quantitative analysis of the levels of p-mTOR$^{(Ser2448)}$. Scale bar = 20 µm (**A**, **D**, **F**), $N = 4$, ns: not significant, $^{*}P < 0.05$, $^{***}P < 0.001$. Rapa, rapamycin.

Investigative Ophthalmology & Visual Science

Rapamycin Further Upregulated PINK1/Parkin-Mediated Mitophagy in the Lacrimal Gland of Middle-Aged Mice

Western blot analysis of lacrimal gland tissue showed that the expression levels of the autophagy-related proteins p62, Beclin-1, and LC3B were significantly upregulated in the middle-aged mice group compared to the control group. The rapamycin treatment showed the highest protein expression level among the three groups ($P < 0.01$ and $P < 0.001$; Fig. 8A). The previous phenomena were further supported by immunofluorescence assay, which showed that the rapamycin treatment group had considerably higher levels of LC3B expression (Fig. 8B). Then, we evaluated the immunofluorescence of LC3B and TOMM20 in lacrimal gland tissues. We found that they co-localized, which suggests that aging induces mitophagy (Fig. 8C). Significantly, the rapamycin treatment group saw a stronger response from this, indicating that rapamycin treatment improved mitophagy. These findings showed that acinar epithelial cells autophagy flux impairment is the cause of aberrant autophagosome accumulation.

To preserve cellular homeostasis and remove damaged mitochondria, cells initiate a mitophagy mechanism in response to numerous physicochemical stressors that cause injury to the mitochondria. In order to investigate whether rapamycin increases mitophagy, double immunofluorescence labeling showed that the aging group expressed much more co-localized of LC3B and Parkin than the control group demonstrated, whereas the rapamycin treatment group expressed substantially more co-localization (Fig. 8D). We also conducted co-localization of TOMM20 and LAMP-1 by immunofluorescence staining, which also showed a similar tendency, indicating that rapamycin increases autophagic flow by restoring lysosome function and fragmenting down unusually large autophagosomes or autolysosomes that had accumulated in acinar epithelial cells (Fig. 8E). Immunofluorescence staining also showed that the lacrimal gland acinar cells revealed a broad co-localization of Parkin and TOMM20 in the middle-aged mice group, rapamycin treatment markedly upregulated the co-localization (Supplementary Fig. S3A). To further investigate mitochondrial dynamics, we investigated the key regulators of mitochondrial fission and fusion MFF, DRP1, and OPA1. We observed an increase in the expression of DRP1 and MFF and a decrease in the expression of OPA1 in the middle-aged mouse group, and a significant upregulation of DRP1 and MFF expression and a significant decrease in OPA1 expression under rapamycin treatment (Supplementary Figs. S3B, S3C). Immunohistochemical assessment revealed that the acinar epithelial cells of the lacrimal gland in rapamycin-treated middle-aged mice expressed OPA1 and DRP1 (Supplementary Figs. S3D, S3E). Compared with control and middle-aged mice, there was a significant increase in positive areas of DRP1 protein and a significant decrease in positive areas of OPA1 protein per visual field in the rapamycin-treated group. Western blot analysis of lacrimal gland tissue showed that the expression levels of the mitophagy-related proteins PINK1 and Parkin were significantly upregulated in the middle-aged mice group, and the tendency could be further upregulated by rapamycin (see Fig. 8A). TEM was used to examine control mice, middle-aged mice, and middle-aged mice with rapamycin treatment. The results were consistent with Western blot analysis and immunofluorescence staining, and an increase in the rapamycin treatment group in the amount of autophagosomes ($P < 0.05$ and $P < 0.001$; Figs. 8F, 8G). Moreover, the lipid droplet of acinar epithelial cells in lacrimal gland tissue was directly observed by TEM, which further confirmed our results ($P < 0.05$ and $P < 0.01$; Figs. 8H, 8I). NaK-ATPase plays a role in the secretion of the lacrimal gland acinar.[39] This was measured by immunofluorescence staining of NaK-ATPase in the lacrimal gland acinar tissue. The results in Supplementary Figure S4A show that the acinar cells stained positive for NaK-ATPase were mostly upregulated in middle-aged mice, whereas the rapamycin treatment significantly reversed it. To observe the myoepithelial cell and progenitors or stem cell changes in the lacrimal gland, we examined the expression of αSMA and p63 in the lacrimal gland. In the middle-aged mice group, αSMA-positive and p63-positive staining cells exhibit reduced in the lacrimal gland than younger counterparts. In contrast, the number of αSMA-positive and p63-positive cells was significantly upregulated in rapamycin-treated middle-aged mice (see Supplementary Fig. S4B). All of these findings suggested that acinar epithelial cells in middle-aged mice have activated PINK1/Parkin-mediated mitophagy, which could be significantly increased by rapamycin.

Inhibition of PINK1/Parkin-Mediated Mitophagy Promoted Histological and Functional Damages in Mouse Lacrimal Gland Acinar

In order to investigate if rapamycin typically reduces acinar epithelial cells mitochondrial damage via activating mitophagy, we added Mdivi-1 to inhibit mitophagy. After treatment with Mdivi-1 to middle-aged mice, we discovered that lacrimal gland tissue damage was shown by H&E staining and Oil O red staining (Figs. 9A, 9B). The results of Masson staining and CD45 staining suggested that markedly increased intracellular collagen in acinar cells, and enhanced infiltration of inflammatory cells in Mdivi-1-treated lacrimal gland acinar cells of middle-aged mice ($P < 0.001$; Figs. 9C, 9D, Supplementary Fig. S5A). Apoptosis was evaluated using TUNEL staining, which indicated that the number of TUNEL-positive cells was significantly upregulated in the Mdivi-1-treated group ($P < 0.001$; Fig. 9E). The Ki67 staining assay indicated that Mdivi-1 interventions can effectively reduce $ki67^+$ cells in the middle-aged model mice ($P < 0.05$; Fig. 9F). The Western blot showed that the expression of p16 and p21 was significantly upregulated in Mdivi-1 treatment middle-aged mice ($P < 0.05$ and $P < 0.001$; Figs. 9G, 9H). Furthermore, we evaluated mitochondrial damage using JC-1 and ROS. As expected, Mdivi-1 significantly increased ROS and an increased shift from red to green fluorescence compared with middle-aged mice ($P < 0.01$ and $P < 0.001$; Figs. 9I, 9L). The TEM results showed that, compared to the middle-aged mice group, Mdivi-1 significantly decreased mitochondrial area and perimeter ($P < 0.05$ and $P < 0.01$; Figs. 9M, 9N). We also found that mtDNA leakage was upregulated in the Mdivi-1 group ($P < 0.001$; Fig. 9O). In addition, CPT1a, CPT2, and C/EBPα were upregulated in Mdivi-1-treated aged mice group (see Supplementary Fig. S5B).

Double immunofluorescence labeling was used to investigate if Mdivi-1 impaired autophagic flow. Compared to the middle-aged group, the Mdivi-1 group had significantly lower LC3B expression, and the p62 expression

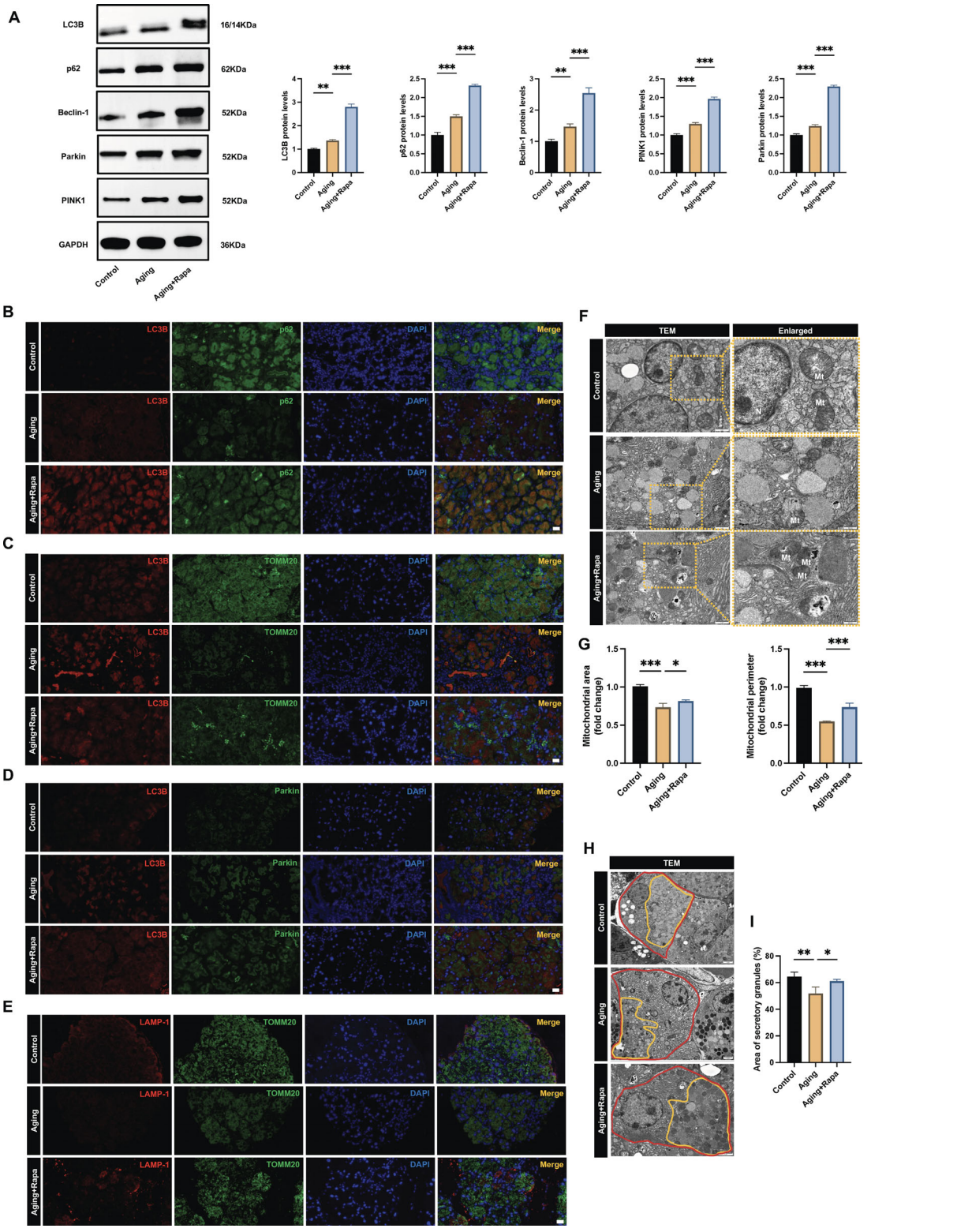

Figure 8. Rapamycin suppresses mitochondrial dysfunction via activating PINK1/Parkin-mediated mitophagy. (**A**) Western blot analysis showed the expression of p62, Beclin-1, LC3B, PINK1, and Parkin in lacrimal gland tissues. (**B**) Immunofluorescence analysis showing the co-localization between LC3B (*red*) and p62 (*green*) in the lacrimal gland, and DAPI (*blue*). (**C**) Immunofluorescence analysis showing the co-localization between LC3B (*red*) and TOMM20 (*green*) in the lacrimal gland, and DAPI (*blue*). (**D**) Immunofluorescence analysis showing the co-localization between LC3B (*red*) and Parkin (*green*) in the lacrimal gland, and DAPI (*blue*). (**E**) Immunofluorescence analysis showing the co-localization between LAMP-1 (*red*) and TOMM20 (*green*) in the lacrimal gland, and DAPI (*blue*). (**F**) Transmission electron microscopy (TEM) images of the ultrastructure of the acinar cells of the lacrimal gland in each group of mice. N, nucleus, Mt, mitochondria. (**G**) Measurement of mitochondrial area and perimeter on the TEM images. (**H**) TEM images of the ultrastructure of the secretory granules in the acinar cells of the lacrimal gland in control and middle-aged lacrimal glands. (**I**) Measurement of secretory granules (marked *yellow*) of acinar cells (marked *red*) on the TEM images. Scale bar = 20 µm (**B**, **C**, **D**, **E**), 1 µm (magnified 500 nm) (**F**, **H**), $N = 4$, $^{*}P < 0.05$, $^{**}P < 0.01$, $^{***}P < 0.001$. Rapa, rapamycin.

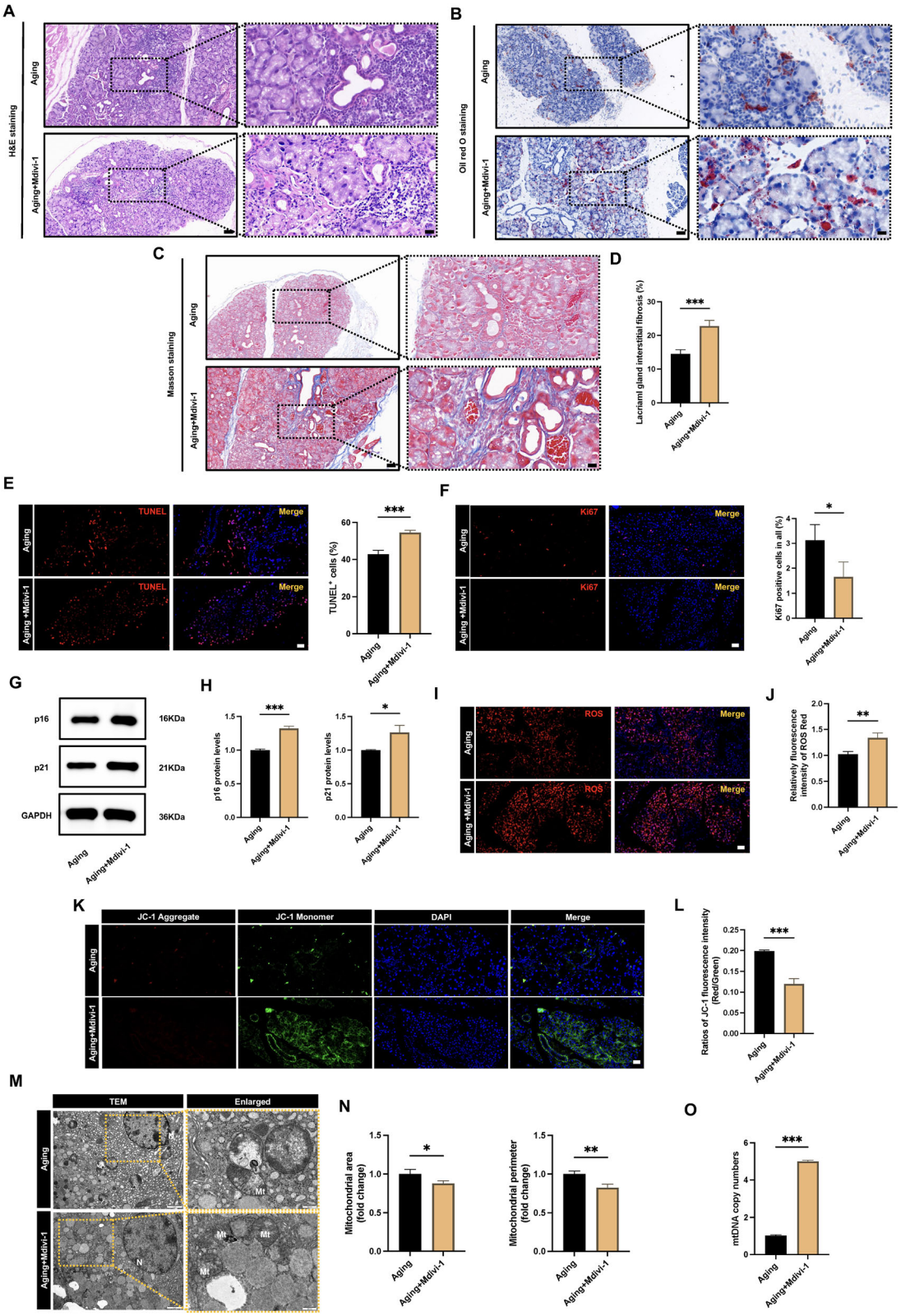

Figure 9. Inhibiting mitophagy aggravated aging-induced lacrimal gland apoptosis and mitochondrial dysfunction. (**A**) Representative images of hematoxylin and eosin (H&E) staining in the lacrimal gland of middle-aged and Mdivi-1 treated middle-aged mice. (**B**) Representative macroscopic images of Oil Red O staining in the lacrimal gland of middle-aged and Mdivi-1 treated middle-aged mice. (**C**) Masson staining shows the lipid droplets in the lacrimal gland of middle-aged and Mdivi-1-treated middle-aged mice. (**D**) Quantitative analysis of the lacrimal gland interstitial fibrosis. (**E**) TUNEL fluorescence staining and quantification results of the lacrimal gland in each group. (**F**) Immunofluorescent staining of Ki67 shows Ki67^{+} cell infiltration in the lacrimal gland of each group of mice. (**G**) Representative Western blot images of p16 and p21 in the lacrimal gland. (**H**) Quantitative analysis of the levels of p16 and p21. (**I**) Immunofluorescence staining

of ROS using ROS probe (*red*) and DAPI (*blue*) in lacrimal gland tissues of control and middle-aged mice. (**J**) Assessment of relative fluorescence intensity of ROS staining. (**K**) Immunofluorescence staining of mitochondrial membrane potential using JC-1 in lacrimal gland tissues of control and middle-aged mice. (**L**) Measurement of relative fluorescence intensity of JC-1 staining. (**M**) Transmission electron microscopy (TEM) images of the ultrastructure of the acinar cells of the lacrimal gland in each group of mice. (**N**) Measurement of mitochondrial area and perimeter on the TEM images. (**O**) Mitochondrial DNA (mtDNA) leakage in the lacrimal gland tissues in the different groups. Scale bar = 50 µm (magnified 20 µm) (**A**, **B**, **C**), 20 µm (**E**, **F**, **I**, **K**), and 1 µm (magnified 500 nm) (**M**), $N = 4$, $^{*}P < 0.05$, $^{**}P < 0.01$, $^{***}P < 0.001$. Rapa, rapamycin.

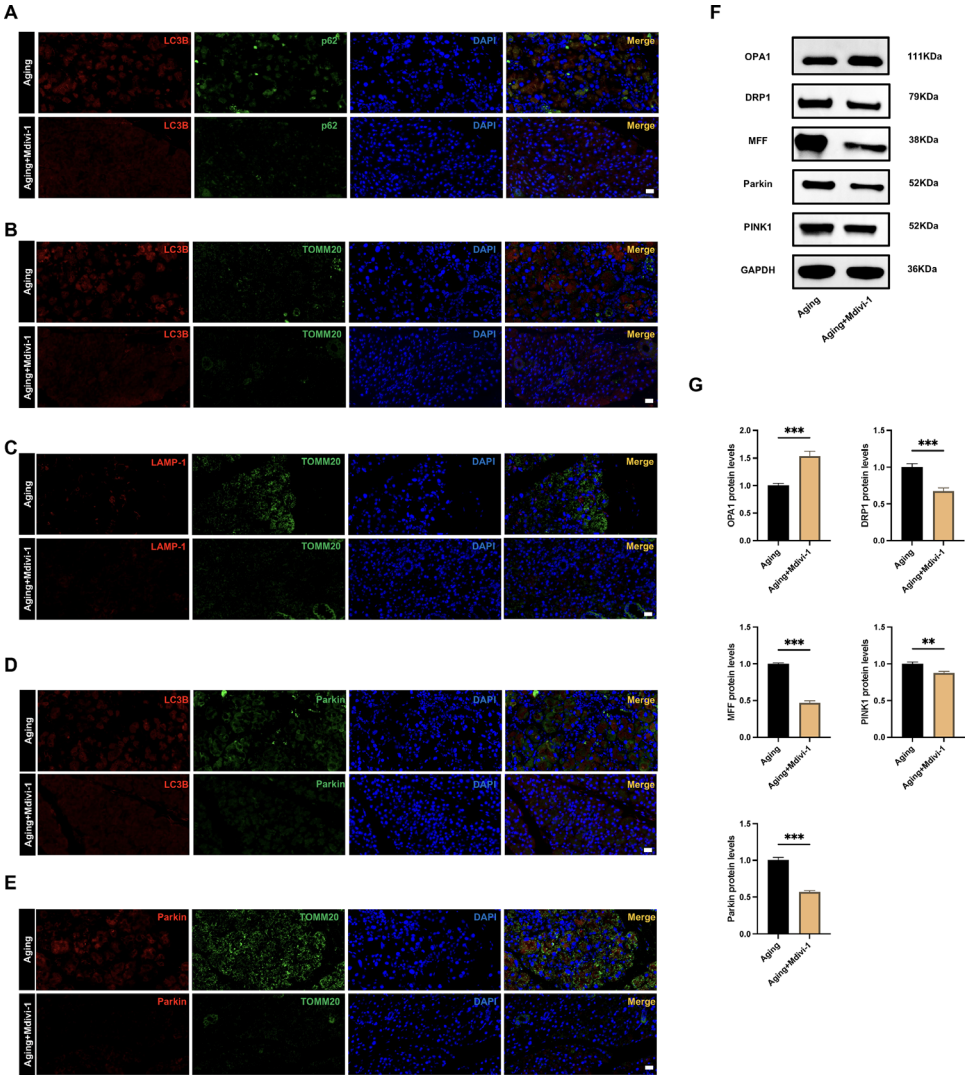

Figure 10. Mdivi-1 inhibits mitophagy-associated PINK1/Parkin activation. (**A**) Immunofluorescence analysis showing the co-localization between LC3B (*red*) and p62 (*green*) in the lacrimal gland, and DAPI (*blue*). (**B**) Immunofluorescence analysis showing the co-localization between LC3B (*red*) and TOMM20 (*green*) in the lacrimal gland, and DAPI (*blue*). (**C**) Immunofluorescence analysis showing the co-localization between LAMP-1 (*red*) and TOMM20 (*green*) in the lacrimal gland, and DAPI (*blue*). (**D**) Immunofluorescence analysis showing the co-localization between LC3B (*red*) and Parkin (*green*) in the lacrimal gland, and DAPI (*blue*). (**E**) Immunofluorescence analysis showing the co-localization between Parkin (*red*) and LAMP-1 (*green*) in the lacrimal gland, and DAPI (*blue*). (**F**) Western blot analysis showed the expression of OPA1, DRP1, MFF, PINK1, and Parkin in lacrimal gland tissues. (**G**) Quantitative analysis of the levels of OPA1, DRP1, MFF, PINK1, and Parkin. Scale bar = 20 µm (**A**, **B**, **C**, **D**, **E**), $N = 4$, $^{**}P < 0.01$, $^{***}P < 0.001$.

was comparatively lower (Fig. 10A). Additionally, compared to the middle-aged mice group, the immunofluorescence results showed a reduction in the co-localization of LC3 and TOMM20 or LAMP-1 and TOMM20 fluorescence after Mdivi-1 treatment (Figs. 10B, 10C). The immunofluorescence staining analysis further demonstrated that Mdivi-1 treatment decreased the colocalization of Parkin with LC3B and TOMM20 in lacrimal gland acinar tissue (Figs. 10D, 10E). This suggests that Mdivi-1 treatment inhibits the degradation of damaged mitochondria by impaired lysosome function. Meanwhile, we analyzed the expression levels of mitochondrial fission and fusion proteins and PINK1/Parkin. The results showed that treatment downregulates the protein level of DRP1 and MFF and upregulated the protein level

of OPA1, and the expression of PINK1 and Parkin were significantly different compared to a middle-aged mouse group, which is consistent with the immunofluorescence staining ($P < 0.01$ and $P < 0.001$; Figs. 10F, 10G). The expression of the OPA1 was significantly increased, and the decreased expression of DRP1 in the Mdivi-1 treated group, as shown in Supplementary Figures S5C and S5D. Those results implied that mitophagy might be an efficient target for the treatment of aging-related lacrimal gland dysfunction.

Discussion

A chronic functional decrease accompanied by numerous biochemical disruptions is called aging. One of the main indicators of aging is mitochondrial malfunction.[40] It has been shown that a number of variables, such as increased formation of ROS, mtDNA, protein oxidations, aberrant energy metabolism, and decreased mitochondrial biogenesis, cause the deterioration of mitochondrial function with age.[41,42] Oxidative damage increases and the capacity of the body to neutralize ROS decreases with age.[43] Continuous ROS generation has the potential to alter biomolecular structures and enzyme functions.[44] Oxidative stress is accelerated by imbalanced ROS creation and neutralization; conversely, ROS generation can be induced by oxidative stress.[45] It has been suggested that oxidative stress causes DNA damage, cellular senescence, and inflammation, which all contribute to the pathophysiology of various disorders.[46]

Because the mitochondria are the main location where ROS are produced, alterations in mitochondrial function can have a major effect on oxidative stress. Age-related changes in mitochondrial activity result in a rise in ROS production. Complex II is in control of producing superoxide anion; respiratory chain complexes I and III take part in the ubiquinone cycle to promote univalent oxygen reduction.[47] Excessive ROS continuously build up in mitochondria throughout aging, which reduces ATP synthesis and disturbs respiratory chain function, ultimately resulting in mitochondrial malfunction and damage.[48] In this study, it has been demonstrated that aging may cause lacrimal gland acinar cells to produce a large amount of ROS, reduce mitochondrial membrane potential, and damage mitochondria, all of which can finally result in cell death.

In recent years, several research have been conducted to investigate the role of mitophagy in connection to aging.[49] Mitophagy is a response of mitochondria to a variety of stresses, including oxidative stress, nutrient starvation, or programmed removal of mitochondria, and senescence impairs mitochondrial function and mitophagy.[50,51] Under healthy settings, the outer/inner mitochondrial membrane complex's translocase imports PINK1, which is subsequently broken down by mitochondrial proteases. When under stress, the depolarized PINK1 of the outer mitochondrial membrane is inhibited, which attracts cytosolic ubiquitin and parkin. Parkin is phosphorylated by PINK1, which activates Parkin's E3 ligase activity. After that, the depolarized mitochondria are targeted by activated Parkin, which ubiquitinates the outer mitochondrial substrates.[52] The protective effect of PINK1-mediated mitophagy against mitochondrial dysfunction has been reported.[53] For instance, in mice models of Alzheimer's disease, the expression level of PINK1/Parkin significantly decreased when compared with control.[54] A significant decrease in the expression level of PINK1/Parkin was found in osteoarthritic rats.[55] As a result, mitophagy may be applied as a therapeutic strategy. However, several research indicates that by stimulating the PINK/Parkin pathway, mitophagy could accelerate aging.[56,57] The disparity might be caused by the degree of mitophagy in various conditions. According to Yamamuro et al. excessive mitophagy may decrease mitochondrial function, which in turn accelerates the aging process. However, mitophagy assists in the removal of damaged mitochondria.[58] In this work, we observed that increased levels of mitophagy may protect lacrimal gland acinar epithelial cells from aging-induced apoptosis by eliminating damaged mitochondria and reducing excessive ROS generation, hence increasing tear secretion. The level of senescence-induced mitophagy appears to be insufficient to prevent lacrimal gland acinar epithelial cells from suffering ROS damage. Thus, when rapamycin strengthens the capacity to conduct mitophagy, the damage of ROS may be reduced.

Targeting mitophagy with pharmaceutical treatments has attracted a lot of attention and might have a big impact on translation. Research suggests that mitophagy stimulation may benefit other glial cells and non-neuronal cells by identifying a protective role for mitophagy in neurons and microglia.[59] To alter the mitophagy signaling pathways or specifically target the mitophagy proteins, a variety of methods are used. According to some research, activating the PINK1/Parkin pathway to enhance mitophagy may be a viable treatment option for Parkinson's disease.[60] By initiating PINK1/Parkin-mediated mitophagy, metformin, a naturally occurring SIRT1-activating substance, has anti-aging properties.[61] By blocking mTOR and increasing PINK1, Parkin, and the pro-autophagic protein BECN1, rapamycin stimulates mitophagy.[62] Research suggests that rapamycin reduces lacrimal gland inflammation and improves ocular surface integrity in mice models of Sjögren's syndrome-associated dry eye.[63] According to prior findings, rapamycin triggers the activation of PINK1/Parkin-mediated mitophagy and alleviates age-related osteoporosis.[64] Notably, utilizing Mdivi-1 to suppress Drp1 causes mitochondrial damage, including an increase in ROS aggregation and a reduction in ATP synthesis. Additionally, Mdivi-1 was observed to worsen ischemic stroke injury in vivo experiments.[65] We explored at the colocalization of autophagy and mitochondria in order to understand more about the function of mitochondrial fission and its relationship to mitophagy. We discovered that whereas Mdivi-1 drastically decreased colocalization. We discovered that whereas Mdivi-1 drastically decreased expression of PINK1/Parkin. Previous study also indicated that treatment with Mdivi-1 significantly decreased the amount of Drp1 translocated into the mitochondria, inhibited PINK1/Parkin-mediated mitophagy, aggregated metabolic cardiomyopathy symptoms, prolonged the course of the illness, and increased its severity.[66]

Conclusions

In summary, we discovered that PINK1/Parkin-mediated mitophagy might prevent aging-induced lacrimal gland acinar epithelial cells apoptosis by removing damaged mitochondria and scavenging ROS, hence preventing the degradation of lacrimal gland microstructural integrity. Treatments that increase mitophagy may protect lacrimal gland acinar epithelial cells damage by maintaining their mitochondrial activity.

Investigative Ophthalmology & Visual Science

Acknowledgments

Supported by National Natural Science Foundation of China (82401225 to Han Zhao) and Natural Science Foundation of Hunan Provincial (2024JJ6587 to Han Zhao).

Authorship Contributions: Han Zhao: Visualization, Validation, Software, Methodology, Investigation, Formal analysis, Funding acquisition, Writing. Yue Zhang: Validation, Methodology, Investigation, Data curation. Yujie Ren: Validation, Methodology, Investigation. Wanpeng Wang: Writing – review & editing, Writing – original draft, Supervision, Methodology, Resources, Project administration, Conceptualization.

Data Availability Statements: The data in this study are available from the corresponding author upon request.

Disclosure: **H. Zhao**, None; **Y. Zhang**, None; **Y.J. Ren**, None; **W.P. Wan**, None

References

1. Dzau VJ, Inouye SK, Rowe JW, Finkelman E, Yamada T. Enabling healthful aging for all - the National Academy of Medicine Grand Challenge in Healthy Longevity. *N Engl J Med*. 2019;381:1699–1701.
2. Gipson IK. Age-related changes and diseases of the ocular surface and cornea. *Invest Ophthalmol Vis Sci*. 2013;54:Orsf48–Orsf53.
3. Campisi J, Kapahi P, Lithgow GJ, Melov S, Newman JC, Verdin E. From discoveries in ageing research to therapeutics for healthy ageing. *Nature*. 2019;571:183–192.
4. Ding J, Sullivan DA. Aging and dry eye disease. *Exp Gerontol*. 2012;47:483–490.
5. Gogola A, Jan NJ, Brazile B, et al. Spatial patterns and age-related changes of the collagen crimp in the human cornea and sclera. *Invest Ophthalmol Vis Sci*. 2018;59:2987–2998.
6. Yazdani M, Elgstøen KBP, Rootwelt H, Shahdadfar A, Utheim ØA, Utheim TP. Tear metabolomics in dry eye disease: a review. *Int J Mol Sci*. 2019;20:3755.
7. The epidemiology of dry eye disease: report of the Epidemiology Subcommittee of the International Dry Eye WorkShop (2007). *Ocul Surf*. 2007;5:93–107.
8. Liu ZG. Emphasis on standardization and refinement in the diagnosis and treatment of dry eye. *Zhonghua Yan Ke Za Zhi*. 2017;53:641–644.
9. Yu J, Asche CV, Fairchild CJ. The economic burden of dry eye disease in the United States: a decision tree analysis. *Cornea*. 2011;30:379–387.
10. Kitazawa K, Inomata T, Shih K, et al. Impact of aging on the pathophysiology of dry eye disease: a systematic review and meta-analysis. *Ocul Surf*. 2022;25:108–118.
11. Rocha EM, Alves M, Rios JD, Dartt DA. The aging lacrimal gland: changes in structure and function. *Ocul Surf*. 2008;6:162–174.
12. de Souza RG, de Paiva CS, Alves MR. Age-related autoimmune changes in lacrimal glands. *Immune Netw*. 2019;19:e3.
13. Ríos JD, Horikawa Y, Chen LL, et al. Age-dependent alterations in mouse exorbital lacrimal gland structure, innervation and secretory response. *Exp Eye Res*. 2005;80:477–491.
14. Obata H, Yamamoto S, Horiuchi H, Machinami R. Histopathologic study of human lacrimal gland. Statistical analysis with special reference to aging. *Ophthalmology*. 1995;102:678–686.
15. Zoukhri D. Effect of inflammation on lacrimal gland function. *Exp Eye Res*. 2006;82:885–898.
16. Guo Y, Guan T, Shafiq K, et al. Mitochondrial dysfunction in aging. *Ageing Res Rev*. 2023;88:101955.
17. Yu T, Slone J, Liu W, et al. Premature aging is associated with higher levels of 8-oxoguanine and increased DNA damage in the Polg mutator mouse. *Aging Cell*. 2022;21:e13669.
18. Ma K, Chen G, Li W, Kepp O, Zhu Y, Mitophagy Chen Q., Mitochondrial homeostasis, and cell fate. *Front Cell Dev Biol*. 2020;8:467.
19. Bakeeva LE, Eldarov CM, Vangely IM, Kolosova NG, Vays VB. Mitochondria-targeted antioxidant SkQ1 reduces age-related alterations in the ultrastructure of the lacrimal gland. *Oncotarget*. 2016;7:80208–80222.
20. Glick D, Barth S, Macleod KF. Autophagy: cellular and molecular mechanisms. *J Pathol*. 2010;221:3–12.
21. Zhang R, Zhu Z, Ma Y, et al. Rhizoma Alismatis Decoction improved mitochondrial dysfunction to alleviate SASP by enhancing autophagy flux and apoptosis in hyperlipidemia acute pancreatitis. *Phytomedicine*. 2024;129:155629.
22. Ajoolabady A, Chiong M, Lavandero S, Klionsky DJ, Ren J. Mitophagy in cardiovascular diseases: molecular mechanisms, pathogenesis, and treatment. *Trends Mol Med*. 2022;28:836–849.
23. Ashrafi G, Schwarz TL. The pathways of mitophagy for quality control and clearance of mitochondria. *Cell Death Differ*. 2013;20:31–42.
24. Sukhorukov V, Voronkov D, Baranich T, Mudzhiri N, Magnaeva A, Illarioshkin S. Impaired mitophagy in neurons and glial cells during aging and age-related disorders. *Int J Mol Sci*. 2021;22:10251.
25. Lou G, Palikaras K, Lautrup S, Scheibye-Knudsen M, Tavernarakis N, Fang EF. Mitophagy and neuroprotection. *Trends Mol Med*. 2020;26:8–20.
26. Zou M, Wang D, Chen Y, Yang C, Xu S, Dai Y. Dajianzhong decoction ameliorated D-gal-induced cognitive aging by triggering mitophagy in vivo and in vitro. *J Ethnopharmacol*. 2024;319:117212.
27. Zhang L, Pitcher LE, Yousefzadeh MJ, Niedernhofer LJ, Robbins PD, Zhu Y. Cellular senescence: a key therapeutic target in aging and diseases. *J Clin Invest*. 2022;132:e158450.
28. Basisty N, Kale A, Jeon OH, et al. A proteomic atlas of senescence-associated secretomes for aging biomarker development. *PLoS Biol*. 2020;18:e3000599.
29. Coppé JP, Patil CK, Rodier F, et al. Senescence-associated secretory phenotypes reveal cell-nonautonomous functions of oncogenic RAS and the p53 tumor suppressor. *PLoS Biol*. 2008;6:2853–2868.
30. Sato S, Ogawa Y, Shimizu E, et al. Cellular senescence promotes meibomian gland dysfunction in a chronic graft-versus-host disease mouse model. *Ocul Surf*. 2024;32:198–210.
31. Yang B, Dan X, Hou Y, et al. NAD(+) supplementation prevents STING-induced senescence in ataxia telangiectasia by improving mitophagy. *Aging Cell*. 2021;20:e13329.
32. Laberge RM, Sun Y, Orjalo AV, et al. MTOR regulates the pro-tumorigenic senescence-associated secretory phenotype by promoting IL1A translation. *Nat Cell Biol*. 2015;17:1049–1061.
33. Herranz N, Gallage S, Mellone M, et al. mTOR regulates MAPKAPK2 translation to control the senescence-associated secretory phenotype. *Nat Cell Biol*. 2015;17:1205–1217.
34. Choi M, Toscano C, Edman MC, de Paiva CS, Hamm-Alvarez SF. The aging lacrimal gland of female C57BL/6J mice exhibits multinucleate macrophage infiltration associated with lipid dysregulation. *Invest Ophthalmol Vis Sci*. 2024;65:1.
35. He J, Zheng F, Zhang L, et al. Single-cell RNA-sequencing reveals the transcriptional landscape of lacrimal gland in GVHD mouse model. *Ocul Surf*. 2024;33:50–63.

Investigative Ophthalmology & Visual Science

36. Huang D, Jiao X, Huang S, et al. Analysis of the heterogeneity and complexity of murine extraorbital lacrimal gland via single-cell RNA sequencing. *Ocul Surf*. 2024;34:60–95.
37. Liu J, Si H, Huang D, et al. Mechanisms of extraorbital lacrimal gland aging in mice: an integrative analysis of the temporal transcriptome. *Invest Ophthalmol Vis Sci*. 2023;64:18.
38. Tang Y, Dou S, Wei C, et al. Single-nuclei characterization of lacrimal gland in scopolamine-induced dry eye disease. *Invest Ophthalmol Vis Sci*. 2024;65:46.
39. Dipolo R, Marty A. Measurement of Na-K pump current in acinar cells of rat lacrimal glands. *Biophys J*. 1989;55:571–574.
40. Hernandez-Segura A, Nehme J, Demaria M. Hallmarks of cellular senescence. *Trends Cell Biol*. 2018;28:436–453.
41. Amorim JA, Coppotelli G, Rolo AP, Palmeira CM, Ross JM, Sinclair DA. Mitochondrial and metabolic dysfunction in ageing and age-related diseases. *Nat Rev Endocrinol*. 2022;18:243–258.
42. Natarajan V, Chawla R, Mah T, et al. Mitochondrial dysfunction in age-related metabolic disorders. *Proteomics*. 2020;20:e1800404.
43. Stefanatos R, Sanz A. The role of mitochondrial ROS in the aging brain. *FEBS Lett*. 2018;592:743–758.
44. Checa J, Aran JM. Reactive oxygen species: drivers of physiological and pathological processes. *J Inflamm Res*. 2020;13:1057–1073.
45. Wei YH, Lee HC. Oxidative stress, mitochondrial DNA mutation, and impairment of antioxidant enzymes in aging. *Exp Biol Med (Maywood)*. 2002;227:671–682.
46. Zhu Y, Armstrong JL, Tchkonia T, Kirkland JL. Cellular senescence and the senescent secretory phenotype in age-related chronic diseases. *Curr Opin Clin Nutr Metab Care*. 2014;17:324–328.
47. Giorgi C, Marchi S, Simoes ICM, et al. Mitochondria and reactive oxygen species in aging and age-related diseases. *Int Rev Cell Mol Biol*. 2018;340:209–344.
48. Zorov DB, Juhaszova M, Sollott SJ. Mitochondrial reactive oxygen species (ROS) and ROS-induced ROS release. *Physiol Rev*. 2014;94:909–950.
49. De Gaetano A, Gibellini L, Zanini G, Nasi M, Cossarizza A, Pinti M. Mitophagy and oxidative stress: the role of aging. *Antioxidants (Basel)*. 2021;10:794.
50. Bakula D, Scheibye-Knudsen M. MitophAging: mitophagy in aging and disease. *Front Cell Dev Biol*. 2020;8:239.
51. Tyrrell DJ, Blin MG, Song J, Wood SC, Goldstein DR. Aging impairs mitochondrial function and mitophagy and elevates interleukin 6 within the cerebral vasculature. *J Am Heart Assoc*. 2020;9:e017820.
52. Pickles S, Vigié P, Youle RJ. Mitophagy and quality control mechanisms in mitochondrial maintenance. *Curr Biol*. 2018;28:R170–R185.
53. Wang Y, Shen J, Chen Y, et al. PINK1 protects against oxidative stress induced senescence of human nucleus pulposus cells via regulating mitophagy. *Biochem Biophys Res Commun*. 2018;504:406–414.
54. Xie C, Zhuang XX, Niu Z, et al. Amelioration of Alzheimer's disease pathology by mitophagy inducers identified via machine learning and a cross-species workflow. *Nat Biomed Eng*. 2022;6:76–93.
55. Jin Z, Chang B, Wei Y, et al. Curcumin exerts chondroprotective effects against osteoarthritis by promoting AMPK/PINK1/Parkin-mediated mitophagy. *Biomed Pharmacother*. 2022;151:113092.
56. Huang D, Peng Y, Li Z, et al. Compression-induced senescence of nucleus pulposus cells by promoting mitophagy activation via the PINK1/PARKIN pathway. *J Cell Mol Med*. 2020;24:5850–5864.
57. Zha Z, Wang J, Wang X, Lu M, Guo Y. Involvement of PINK1/Parkin-mediated mitophagy in AGE-induced cardiomyocyte aging. *Int J Cardiol*. 2017;227:201–208.
58. Yamamuro T, Kawabata T, Fukuhara A, et al. Age-dependent loss of adipose Rubicon promotes metabolic disorders via excess autophagy. *Nat Commun*. 2020;11:4150.
59. Fang EF, Hou Y, Palikaras K, et al. Mitophagy inhibits amyloid-β and tau pathology and reverses cognitive deficits in models of Alzheimer's disease. *Nat Neurosci*. 2019;22:401–412.
60. Pickrell AM, Youle RJ. The roles of PINK1, parkin, and mitochondrial fidelity in Parkinson's disease. *Neuron*. 2015;85:257–273.
61. Wang C, Yang Y, Zhang Y, Liu J, Yao Z, Zhang C. Protective effects of metformin against osteoarthritis through upregulation of SIRT3-mediated PINK1/Parkin-dependent mitophagy in primary chondrocytes. *Biosci Trends*. 2019;12:605–612.
62. Mahalakshmi R, Priyanga J, Bhakta-Guha D, Guha G. Hormetic effect of low doses of rapamycin triggers anti-aging cascades in WRL-68 cells by modulating an mTOR-mitochondria cross-talk. *Mol Biol Rep*. 2022;49:463–476.
63. Shah M, Edman MC, Reddy Janga S, et al. Rapamycin eye drops suppress lacrimal gland inflammation in a murine model of Sjögren's syndrome. *Invest Ophthalmol Vis Sci*. 2017;58:372–385.
64. Li W, Jiang WS, Su YR, et al. PINK1/Parkin-mediated mitophagy inhibits osteoblast apoptosis induced by advanced oxidation protein products. *Cell Death Dis*. 2023;14:88.
65. Wu Q, Liu J, Mao Z, et al. Ligustilide attenuates ischemic stroke injury by promoting Drp1-mediated mitochondrial fission via activation of AMPK. *Phytomedicine*. 2022;95:153884.
66. Huang JR, Zhang MH, Chen YJ, et al. Urolithin A ameliorates obesity-induced metabolic cardiomyopathy in mice via mitophagy activation. *Acta Pharmacol Sin*. 2023;44:321–331.

Investigative Ophthalmology & Visual Science